การกำจัดมลพิษสีด้วยท่อคาร์บอนระดับนาโนเมตรแบบผนังหลายชั้นที่มีสมบัติแม่เหล็ก

นายณัฐพล อัครพัทธางกูร

REMOVAL OF DYE POLLUTANTS USING MULTI-WALLED CARBON NANOTUBES WITH MAGNETIC CHARACTERISTICS

Mr. Nattapol Akrapattangkul

Thesis Title   REMOVAL OF DYE POLLUTANTS USING MULTI-
                   WALLED CARBON NANOTUBES WITH MAGNETIC
                   CHARACTERISTICS
By   Mr. Nattapol Akrapattangkul
Field of Study   Chemical Engineering
Thesis Advisor   Associate Professor Tawatchai Charinpanitkul, D.Eng.
Thesis Co-advisor Apinan Soottitantawat, D.Eng.

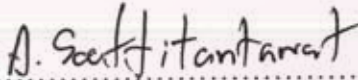---

Accepted by the Faculty of Engineering, Chulalongkorn University in
Partial Fulfillment of the Requirements for the Master's Degree

....Dean of the Faculty of Engineering
(Associate Professor Boonsom Lerdhirunwong, Dr.Ing.)
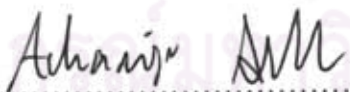
THESIS COMMITTEE

.... Chairman
(Professor Suttichai Assabumrungrat, Ph.D.)

.... Thesis Advisor
(Associate Professor Tawatchai Charinpanitkul, D.Eng.)

.... Thesis Co-advisor
(Apinan Soottitantawat, D.Eng.)

.... Examiner
(Assistant Professor Varong Pavarajarn, Ph.D.)

.... Examiner
(Achariya Suriyawong, Ph.D.)

.... External Examiner
(Kajornsak Faungnawakij, D.Eng.)

ณัฐพล อัครพัทธางกูร: การกำจัดมลพิษสีด้วยท่อคาร์บอนระดับนาโนเมตรแบบผนัง
หลายชั้นที่มีสมบัติแม่เหล็ก. (REMOVAL OF DYE POLLUTANTS USING
MULTI-WALLED CARBON NANOTUBES WITH MAGNETIC
CHARACTERISTICS) อ. ที่ปรึกษาวิทยานิพนธ์หลัก: รศ.ดร .ธวัชชัย ชรินพาณิช
กุล, อ.ที่ปรึกษาวิทยานิพนธ์ร่วม: อ.ดร. อภินันท์ สุทธิธารธวัช, 87 หน้า.

อนุภาคคาร์บอนในระดับนาโนเมตรที่มีโลหะเหล็กเป็นองค์ประกอบภายในชั้นของ
แกรไฟต์สามารถสังเคราะห์ได้ด้วยวิธีการไพโรไลซิสร่วมของของผสมระหว่างเฟอโรซีนและแนฟ
ทาลี โดยอนุภาคที่สังเคราะห์ได้นั้นประกอบด้วย ท่อนาโนคาร์บอนระดับนาโนเมตร และคาร์บอนนา
โนแคปซูล ในงานวิจัยนี้อนุภาคที่สังเคราะห์ได้ถูกนำมาใช้ในการจำกัดสีย้อมสังเคราะห์ในน้ำเสีย
จำลอง ทั้งนี้อนุภาคเหล็กระดับนาโนเมตรถูกหุ้มอยู่ในชั้นแกรไฟต์สามารถตอบสนองต่อ
สนามแม่เหล็กภายนอกส่งผลให้สามารถแยกเก็บอนุภาคที่แขวนลอยอยู่ในสารละลายด้วย
สนามแม่เหล็ก

ในงานวิจัยนี้ได้ทำการศึกษาถึงอิทธิพลของเวลาในการดูดซับ   ความเข้มข้นเริ่มต้นของ
สารละลายสีย้อม ปริมาณอนุภาคคาร์บอนระดับนาโนเมตรที่ใช้เป็นตัวดูดซับ และ ค่าความเป็นกรด-
ด่างเริ่มต้นของสารละลายต่อสมรรถภาพการดูดซับบนอนุภาคคาร์บอนระดับนาโนเมตร ปริมาณการ
ดูดซับสูงสุดของสีย้อมชนิด แมททิลีนบลู รีแอ็คทีฟ เรด31 และ รีแอ็คทีฟ แบล็ค5 เท่ากับ 22.11 34.26
และ 84.94 มิลลิกรัมต่อกรัมตัวดูดซับ ตามลำดับ ทั้งยังศึกษาถึงสมดุลและจลนพลศาสตร์การดูดซับ
โดยพบว่า   จลนพลศาสตร์ของการดูดซับเป็นไปตามแบบจำลองทางคณิตศาสตร์จลนพลศาสตร์การ
ดูดซับอันดับสองเสมือน และ สมดุลการดูดซับเป็นไปตามแบบจำลองสมดุลการดูดซับของฟรุนดริช

อนุภาคคาร์บอนระดับนาโนเมตรที่สังเคราะห์แสดงข้อดีของการเป็นตัวดูดซับระบบการดูด
ซับ   คือ   การที่อนุภาคคาร์บอนระดับนาโนเมตรมีความง่ายในการแยกออกจากสารละลายด้วย
สนามแม่เหล็ก และ การคืนสภาพด้วยสารละลายกรดตัวอย่าง พบว่า ค่าความจุการดูดซับของแมททิลี
นบลู รีแอ็คทีฟ เรด31 และ รีแอ็คทีฟ แบล็ค5 ด้วยอนุภาคคาร์บอนในระดับนาโนเมตรในการดูดซับ
ภายหลังการคืนสภาพรอบที่สามมีค่าเท่ากับ 20.7, 19.8 และ 60.0 มิลลิกรัมต่อกรัมตัวดูดซับ
ตามลำดับ

ภาควิชา	วิศวกรรมเคมี	ลายมือชื่อนิสิต	
สาขาวิชา	วิศวกรรมเคมี	ลายมือชื่อ อ.ที่ปรึกษาวิทยานิพนธ์หลัก	
ปีการศึกษา	2553	ลายมือชื่อ อ.ที่ปรึกษาวิทยานิพนธ์ร่วม	

5170564621   : MAJOR CHEMICAL ENGINEERING
KEYWORDS: CARBON NANOTUBES / DYE REMOVAL / ADSORPTION

NATTAPOL AKRAPATTANGKUL : REMOVAL OF DYE POLLUTANTS USING MULTI-WALLED CARBON NANOTUBES WITH MAGNETIC CHARACTERISTICS. ADVISOR: ASSOC. PROF. TAWATCHAI CHARINPANITKUL, D.Eng., CO-ADVISOR : APINAN SOOTITANTAWAT, D.Eng., 87 pp.

Carbon nanoparticles (CNPs) which are multi-walled carbon nanotubes (MWCNTs) and multi-shell carbon nanocapsules (CNCs) could be synthesized by co-pyrolysis of ferrocene/glycerol mixture. They are utilized for removal of synthetic dyes dispersed in aqueous solutions. The synthesized CNPs which containing Fe-nanoparticles could be collected from the suspension by applying external magnetic field.

In this research the effects of contact time, initial dye concentration, CNPs adsorbent dosage and initial pH value of dye solutions on dye adsorption performance are comprehensively investigated. The maximum adsorption capacities are 22.11, 34.26 and 84.94 mg/g for Methylene Blue, Reactive Red31 and Reactive Black5, respectively. Adsorption kinetic and adsorption isotherm were examined to get confirmation of the pseudo second-order model and Freundlich adsorption characteristics, respectively.

The synthesized CNPs exhibit main advantages of its simplicity in regeneration with typical acid and recovery by magnetic field. After 3-cycle of adsorption and regeneration, final adsorption capacity of Methylene Blue, Reactive Red31 and Reactive Black5 on the synthesized CNPs is 20.7, 19.8 and 60.0 mg/g , respectively.

ACKNOWLEDGEMENTS

CONTENTS

ศูนย์วิทยทรัพยากร
จุฬาลงกรณ์มหาวิทยาลัย

LIST OF TABLES

LIST OF FIGURES

Page

CHAPTER I
INTRODUCTION

1.1 Introduction

Synthetic dyestuffs are widely used in various fields, such as textiles, leather, paper, plastic, before being discharged into various water sink, leading to a serious environmental problem. The treatment of dye-contaminated wastewater is a concerned issue in many countries. Dye pollutant is a cause of not only mental aesthetic problem but also reducing light photosynthesis which could affect ecological balance. Most of the used-synthetic dyes are stable to photo degradation, bio-degradation and oxidizing agents. Furthermore, it is difficult to remove such dyes using chemical coagulation due to their stability in water.

Therefore, some adsorption processes using carbon materials as adsorbent have been attractive due to various advantages, such as efficiency, effectiveness and simple facility. However, the separation inconvenience is also the main drawback of such process. Magnetic separation is anticipated a good separation system in adsorption process.

Synthesizing carbon nanoparticles (CNPs), particularly carbon nanotubes (CNTs) have attracted a lot of researchers attentions due to their unique structure, chemical and electrical properties as long as they were officially reported by Iijima in 1991 [1]. CNTs can be classified into single-walled carbon nanotubes (SWCNTs) and multi-walled carbon nanotubes (MWCNTs) from the graphene layer. The properties of CNTs can be influenced by surface modification with selected organic, inorganic and biological species. Because of their relatively large specific surface area, small size and excellent in structure, CNTs are recognized as a new promising type of solid-phase adsorbents. However, there are very limited reports on the dye adsorption of CNTs with magnetic property.

There are many methods which have been applied for CNP synthesis, such as laser ablation, arc discharge [2], chemical vapor deposition and pyrolysis [3-8]. Among those methodologies, pyrolysis is recognized as an efficient mean for large-scaled production with low operating costs and possible usage of cheap carbon source, such as anthracene [3], acetylene [4-6], naphthalene [7] or benzene [8] to decrease the amount of expensive ferrocene consumed in the synthesis.

In this work, a simple and efficient method for synthesizing CNPs which including multi-walled carbon nanotubes (MWCNTs) and multi-shell carbon nanocapsules (CNCs) with magnetic characteristics by co-pyrolysis of ferrocene and glycerol will be conducted and then the adsorption of some typical dyes onto the synthesized will thoroughly be investigated. In addition, the regeneration of used MWCNTs which will be separated by magnetic system will also be investigated.

1.2 Objectives

1. To synthesize MWCNTs with a magnetic property by co-pyrolysis of ferrocene and glycerol, and the adsorption of some typical dyes onto the synthesized MWCNTs will be investigated.
2. The regeneration of used MWCNTs which will be separated by magnetic system will also be investigated.

1.3 Scope of research works

The scope of this research is limited in laboratory scale as follows:
1. Preparation of MWCNTs by co-pyrolysis of glycerol and ferrocene with molar ratio of 5:1.
2. Characterization of MWCNT morphology and properties.
3. Dispersion of three typical dyes (Methylene Blue, Reactive Red 31 and Reactive Black 5) in distilled water.

4. Investigation of the dye adsorption performance of the synthesized CNPs.

5. Study the effect of initial concentration of dye solutions in the range of 10-100 mg/L

6. Study the amount of MWCNTs loading in the range of 0.3-0.9 g/L

7. Study the effect of initial pH value of dye solutions in the range of 3-11

8. Investigation of the magnetic separation and the recovery efficiency in water with various pH values.

1.4 Procedures of the research

1. Survey and review related literatures.

2. Prepare chemicals and equipments to be used in this research.

3. Carry out synthesis and characterization of MWCNTs.

4. Carry out experiments under various conditions of adsorption and recovery.

5. Determine suitable condition of dye adsorption.

6. Analyze and conclude the experimental results.

7. Summarize all experimental works and prepare thesis.

1.5 Expected benefits

The expected benefit from this research will be the knowledge in synthesis of MWCNTs by co-pyrolysis and the adsorption of dyes contaminated in water by making use of the synthesized MWCNTs.

CHAPTER II
LITERATURE REVIEW

Regarding to some previous works, basic information of on-going efforts in MWCNT synthesis and its applications could be summarized as follows,

2.1 Synthesized carbon nanoparticles

Hou et al. also reported that single-wall carbon nanotubes (SWCNTs) and well-aligned thin multi-walled carbon nanotubes (MWCNTs) were successfully synthesized via pyrolysis of a powder mixture of ferrocene and anthracene or 9, 10-dibromoanthracene. The size of the MWCNTs can be tuned just by changing the ratio of ferrocene/anthracene in the mixture. A lower ratio resulted in low-diameter MWCNTs containing up to only five graphene layers. However, a high ratio has led to thick MWCNTs with more than 25 layers and the pyrolysis of pure ferrocene in a hydrogen flow that mainly gives rise to metal nanoparticles. When powder mixtures of ferrocene and 9, 10-dibromoanthracene were pyrolyzed, both SWCNTs and spherical carbon-coated iron nanoparticles were obtained [3].

Satishkumar et al. made use of gas-phase pyrolysis of acetylene along with a metallocene or with a binary mixture of metallocenes in a flowing stream of Ar or Ar + H_2 at 1100 °C to synthesize single-walled carbon nanotubes (SWNTs). Pyrolysis of $Fe(CO)_5$-acetylene mixtures in Ar at 1100 °C could give single-walled nanotubes. The diameter of the SWNTs was generally around 1 nm, showing thereby that on pyrolysis under the dilute conditions, the organometallic precursors could give rise to very fine metal particles essential for the formation of SWNTs [4].

Satishkumar et al. prepared aligned nanotube bundles by pyrolysis of ferrocene along with methane, acetylene or butane. Ferrocene–acetylene mixtures were found to be ideal for the production of compact aligned nanotube bundles. The nanotubes bundles were associated with iron nanoparticles of diameters in the range 2–13 nm. These nanoparticles are ferromagnetic, showing low saturation magnetization compared to bulk iron. The ferromagnetism of the transition metal nanoparticles is likely to be responsible for the alignment of the nanotubes [6].

Charinpanitkul et al. showed that co-pyrolysis of ferrocene and naphthalene could be utilized for synthesis of carbon nanoparticles which are carbon nanotubes (CNTs) and carbon nanocapsules (CNCs), which contained Fe particles in their carbon shells, were simultaneously fabricated. Transmission electron microscopy (TEM) and scanning electron microscopy (SEM) analyses revealed that morphology and size of the carbon nanostructure strongly depended on the pyrolysis temperature. At a higher temperature, formation of CNCs would become more enhanced. Particle size distribution and yield of the synthesized products were also significantly influenced by the pyrolysis temperature [7].

Bai et al. synthesized carbon nanostructures by a floating catalyst method. Carbon nanotubes (CNTs) and carbon nanofibers CNFs with different diameters and structures can be obtained by controlling the ferrocene (catalyst precursor)/benzene (carbon source) molar ratio. Nominal diameter of CNFs and CNTs increased while ferrocene/benzene molar ratio was decreased. SWNTs could be synthesized when ferrocene/benzene molar ratio was above 15.1% meanwhile MWNTs could be produced when ferrocene/benzene molar ratio was between 4.2% and 8.76% and CNFs could be synthesized when the ratio of ferrocene/benzene was below 4.2% [8].

Sano et al. showed that Fe-containing CNCs and CNTs were separately formed by pyrolysis of ferrocene in a pure H stream through a cylindrical furnace with a temperature profile controlled at 1050 °C in its center. The CNTs and CNCs were, respectively, formed at the 988 °C zone and colder downstream zone of 625 °C. The CNCs were observed to have an iron carbide core. Typical CNC particle sizes were in the 11–30 nm diameter size range with 2–40 graphitic shells [9].

Lu et al. synthesized carbon-encapsulated Fe nanoparticles via a picric acid-detonation-induced pyrolysis of ferrocene. And they found the nanoparticles exhibit well-constructed core–shell structures, with bcc-Fe cores and graphitic shells and the graphitic shells can protect effectively the cores against the attack of HNO_3 solution. The core–shell nanoparticles are preferably formed at low C/Fe atomic ratios, while tubular structures are formed at high C/Fe ratio. Spheroidal Fe nanoparticles have a narrow diameter distribution of 5–20nm. From XRD analysis they could not found iron carbides in these products. The absence of carbides in these samples is possibly associated with the special high temperature environment [10].

Zhang et al. has recently studied of reaction temperature and duration of the growth of aligned carbon nanotube arrays. Layered aligned multi-wall carbon nanotube (MWNT) films have grown directly by pyrolysis of ferrocene in xylene with the help of cobalt powder. The results indicated that the obtained products composed of many separated layers with MWNTs. The reaction temperature significantly influenced the alignment of the MWNTs, and an appropriate reaction temperature range for growth was 800–900°C. Besides temperature, the reaction duration influenced the length of the well-aligned carbon nanotubes [11].

Kobayashi et al. investigated single-walled carbon nanotube (SWNT) growth using a novel Fe_3O_4 nanoparticle catalyst synthesized with a simple organic chemistry process. Discrete nanoparticles with a uniform diameter of ~4 nm could be deposited on Si substrates with a thermal oxide layer by spin-coating with a nanoparticle solution. These nanoparticles were found to have remarkable catalytic activity in the CVD growth of the SWNTs. SWNTs with diameters of around 1 nm were produced from the reduced nanoparticle catalyst. The diameters of the grown SWNTs were closely correlated with those of the catalytic nanoparticles and tended to be slightly smaller than the particle size [12].

Li et al. have discussed on the growth mechanism which involved in two sizes of iron nanoparticles. While the small particle is catalytically active for the nucleation of the nanotube, the large particle produces the carbon atomistic species required for the growth of the nanotubes. From TEM analysis showed that the diameters of the nanotubes are significantly larger than those of the nanotubes grown at a lower temperature. The aligned nanotubes are believed to be the result of a competition growth process along the normal direction of the substrate. The surface diffusion of carbon atoms on the large iron particle leads to the formation of the observed bamboo-like structure [13].

Lee et al. have grown aligned carbon nanotubes by pyrolysis of ferrocene and acetylene in the temperature range 700–1000°C. As the temperature increases, the growth rate increases by 60 times and the relative amount of crystalline graphitic sheets increases significantly. However, the length of aligned CNTs reaches up to 3 mm at 1000°C. The Arrhenius plot yields the activation energy 35±3 kcal/mol, which is close to the diffusion energy of carbon in bulk γ-Fe. It can be suggested that the bulk diffusion of carbons would play an important role in the growth of cylindrical structured carbon nanotubes [14].

2.2 Application of MWCNTs on removal dye pollutants

Qu et al. prepared MWCNTs filled with Fe_2O_3 nanoparticles via hydrothermal reaction of shortened MWCNTs in ferric nitrate solution and subsequent calcinations. The prepared magnetic MWCNTs can be well dispersed in the water and can be easily magnetic separated from the medium after adsorption. The adsorption capacities for MB and NR in the concentration range studied at pH 6 are 42.3 and 77.5 mg/g, respectively. It is a superior absorbent for the removal of NR and MB from wastewater. Compared with other absorbents, the magnetic nanotubes not only have high adsorption efficiency to dyes, but also can be easily manipulated by external magnetic field [15].

Gong et al. reported that the magnetic MWCNTs nanocomposite adsorbent for effective cationic dye removal has been prepared. The adsorption capacity of the adsorbent towards cationic dyes such as MB, NR and BCB was illustrated by experimental adsorption isotherms at room temperature. The results suggested that the adsorption capacity of three cationic dyes on MMWCNT adsorbent increased with temperature Cationic dyes adsorbed increased with pH due to the electrostatic attraction between the negatively charged MMWCNT adsorbent surface and the positively charged cationic dyes. The prepared magnetic multi-wall carbon nanotubes adsorbent with a surface area ($61.74m^2/g$) displayed the main advantage of separation convenience compared to other adsorbents [16].

Wu investigated the adsorption efficiency of carbon nanotubes for Procion Red MX-5B at various pHs and temperatures. The amount adsorbed increased with the CNTs dosage; however, the adsorption capacity initially increased with the CNTs dosage (<0.25 g/l) and then declined as the CNTs dosage increased further (>0.25 g/l). The linear correlation coefficients and standard deviations of Langmuir and Freundlich isotherms were determined and the results revealed that Langmuir isotherm fitted the experimental results well. Kinetic analyses were conducted using pseudo first and second-order models

and the intraparticle diffusion model. The regression results showed that the adsorption kinetics were more accurately represented by a pseudo second-order model. Moreover, Wu's study suggested that the adsorption of Procion Red MX-5B onto CNTs was physisorption [17].

Kuo et al. reported the feasibility of removing direct dyes Direct Yellow 86 (DY86) and Direct Red 224 (DR224) from aqueous solutions using carbon nanotubes (CNTs). Pseudo second-order and intraparticle diffusion were adopted to evaluate experimental data and thereby elucidate the kinetic adsorption process. Additionally, this study used the Langmuir, Freundlich, Dubinin and Radushkevich (D–R) and Temkin isotherms to describe equilibrium adsorption. The adsorption percentage of direct dyes increased as CNTs dosage and temperature increased. The pseudo second-order model best represented adsorption kinetics. Based on the regressions of intraparticle diffusion model, experimental data suggested that the adsorption of direct dyes onto CNTs involved intraparticle diffusion, but that was not the only rate-controlling step. The equilibrium adsorption of DR86 is best fitted in the Freundlich isotherm and that of DR224 was best fitted in the D– R isotherm. The capacity of CNTs to adsorb DY86 and DR224 was 56.2 and 61.3 mg/g, respectively [18].

Luo and Zhang prepared maghemite nanoparticles with a submerged circulation impinging stream reactor (SCISR).The cellulose beads containning Fe_2O_3 nanoparticles exhibited sensitive magnetic response, and their recovery could facilitate by applying a magnetic field. The adsorption and desorption of the organic dyes on MCB-AC were investigated to evaluate the removal of dyes (methyl orange and methylene blue) with different charges from aqueous solution. Their adsorption kinetics experiments were carried out and the data were well fitted by a pseudo-second-order equation. The results revealed that the MCB-AC sorbent could efficiently adsorb the organic dyes from wastewater, and the used sorbents could be recovered completely [19].

Zhu et al. prepared chitosan wrapping magnetic nanosized γ-Fe$_2$O$_3$ and multi-walled carbon nanotubes (m-CS/γ-Fe$_2$O$_3$/MWCNTs) under relative mild conditions. Adsorption of methyl orange (MO) onto m-CS/γ-Fe$_2$O$_3$/MWCNTs was investigated with respect to pH, initial MO concentration and temperature. Results of characterizations indicated that magnetic nanosized c-Fe2O3 and MWCNTs have been wrapped by crosslinked chitosan. Kinetics data and adsorption isotherm were better fitted by pseudo-second-order kinetic model and by Langmuir isotherm, respectively. After adsorption, m-CS/γ-Fe$_2$O$_3$/MWCNTs could be effectively and fleetly separated by applying a magnetic field [20].

Based on literature reviews, it might be implied that carbon nanoparticles, which was synthesized by thermal co-pyrolysis with the mixture of ferrocene and any carbon sources, are a promising novel solid adsorbent for removal dye pollutants. Furthermore, it could be separated from the aqueous solution by magnetic system due to its magnetic properties.

CHAPTER III
THEORY

3.1 Carbon nanoparticles (CNPs)

Since the first discovery of C_{60}, Buckminsterfullerene, by H. Kroto and R. Smalley in 1985 [21], it has initiated substantial attentions in many research areas particularly those of synthesizing carbon nanoparticles (CNPs) such as nanotubes (CNTs), nanohorns (CNHs), nanocapsules (CNCs) and so on. Among these structures, carbon nanotubes (CNTs) are currently the subject of intense research because of their extraordinary mechanical and electrical properties.

3.1.1 Buckminsterfullerene (C_{60})

60 carbon atoms in C_{60} are located at the vertices of a regular truncated icosahedron, 0.710 nm in diameter. Every carbon site on the C_{60} molecule is equivalent to every other site (see Fig. 3.1). The average nearest neighbor carbon-carbon (C-C) distance in C_{60} is very small (0.144 nm) and is almost identical to that in graphite (0.142 nm). Each carbon atom in C_{60} (and also in graphite) is trigonally bonded to three other carbon atoms, and 20 of the 32 faces on the regular truncated icosahedron are hexagons, the remaining 12 being pentagons. Thus we may consider the C_{60} molecule as a "rolled-up" graphene sheet (a single layer of crystalline graphite) which forms a closed shell molecular nanostructure, in keeping with Euler's theorem, which states that a closed surface consisting of hexagons and pentagons has exactly 12 pentagons and an arbitrary number of hexagons. The introduction of pentagons gives rise to curvature in forming a closed surface. To minimize local curvature, the pentagon become separated from each other in the self-assembly process, giving rise to the isolated pentagon rule, an important rule for stabilizing fullerene clusters.
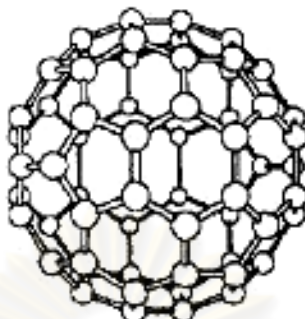
Figure 3.1 Structure of C_{60}, Buckminsterfullerene [22]

3.1.2 Carbon nanotubes (CNTs)

Carbon nanotubes (CNTs) are a very new allotrope of carbon. Carbon nanotubes can be described as graphene sheet rolled into a cylindrical shape. The chemical bonding of carbon nanotubes are composed entirely of sp^2 bonds, similar to those of graphite.

There are two main types of carbon nanotubes; single-walled carbon nanotubes (SWCNTs) and multi-walled carbon nanotubes (MWCNTs) are following these; SWCNTs can be conceptualized by wrapping a one-atom-thick layer of graphite called graphene into a seamless cylinder which is shown in Figure 3.2(a). Meanwhile, MWCNTs consist of multiple layers of graphite rolled in on themselves to form a tube shape which is shown in Figure 3.2(b).

Interestingly, these nested tubes exhibit interlayer spacings of 3.4 A°, a value that is slightly greater than that of graphite (3.35 A°). Iijima attributed this difference to a combination of the tubule curvature and van der Waals interactions between the successive cylinders. Theoretically, it is possible to construct a carbon tube by rolling up a hexagonal graphene sheet in various ways. Two of these are 'non-chiral', so that the honeycomb lattices located at the top and bottom of the tube are always parallel. These configurations are known as 'armchair' and 'zigzag'. In the armchair structure, two C–C bonds on opposite sides of each hexagon are perpendicular to the tube axis, whereas, in the zigzag arrangement, these bonds are parallel to the tube axis (Fig. 3.3, b). All other conformations, where the C–C bonds lie at an angle to the tube axis, are known as 'chiral' or helical structures (Fig. 3.3 c).
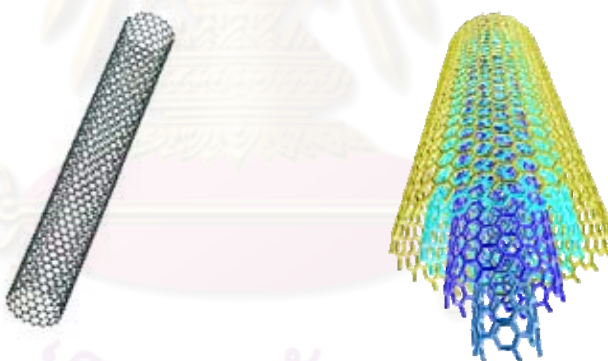
Fig. 3.2 Structure of carbon nanotubes (a) SWCNTs and (b) MWCNTs
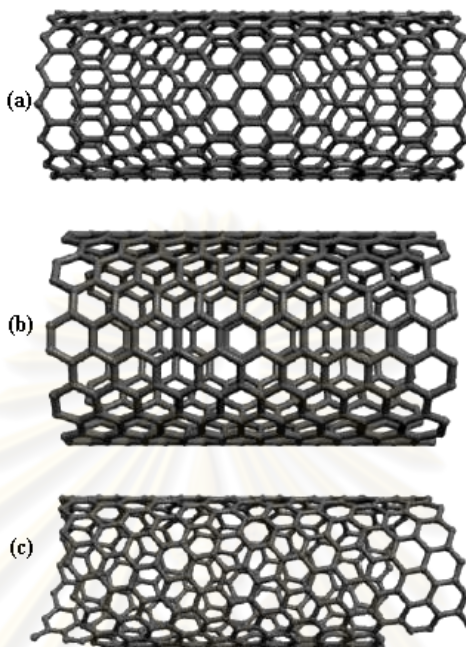
Figure 3.3 Molecular models of SWCNT exhibiting different chiralities
a) zigzag arrangement; b) armchair configuration; c) chiral conformation

At present, carbon nanotubes can be obtained using various techniques: arc discharge, pyrolysis of hydrocarbons over catalysts, laser and solar vaporization, and electrolysis. These nanoscale materials can exhibit different morphologies such as straight, curled, hemitoroidal, branched, spiral, helix-shaped, etc. In 1992, two groups predicted theoretically that single-walled carbon nanotubes (SWNTs) might be metallic or semiconducting carbon nanowires, depending upon their helicity and diameter.

Recent examples of applications include the use of carbon nanotubes as:

- gas storage components of argon, nitrogen, and hydrogen
- AFM probes and field emission sources
- high power electrochemical capacitors
- chemical sensors
- magnetic data storage (e.g. iron filled nanotubes)
- nanocomposites, etc.

They exhibit extraordinary strength and unique electrical properties. Information of attraction properties of CNTs could be briefly summarized as follows,

- Strength property

Carbon nanotubes are one of the strongest and stiffest materials known, in terms of tensile strength and elastic modulus, respectively. This strength results from the covalent sp^2 bonds formed between the individual carbon atoms. A multi-walled carbon nanotube was tested to have a tensile strength of 63 GPa . In comparison, high-carbon steel has a tensile strength of approximately 1.2 GPa. Further, CNTs have very high elastic modulus, on the order of 1 TPa.

- Electrical property

Because of the symmetry and unique electronic structure of graphene, the structure of a nanotube strongly affects its electrical properties. In theory, metallic nanotubes can have an electrical current density more than 1,000 times greater than metals such as silver and copper.

- Thermal property

All nanotubes are expected to be very good thermal conductors along the tube, exhibiting a property known as "ballistic conduction," but good insulators laterally to the tube axis. It is predicted that carbon nanotubes will be able to transmit up to 6000 watts per meter per Kelvin at room temperature; comparing to copper, a metal well-known for its good thermal conductivity, which only transmits 385 watts per meter per Kelvin [14].

From these properties, carbon nanotubes have potentially useful in many applications in nanotechnology, electronics, optics and other fields of materials science. Many techniques have been developed to produce nanotubes in sizeable quantities, including arc discharge, laser ablation and pyrolysis of carbon-containing molecules. Comparison of these techniques, pyrolysis could be a possibility to produce nanotubes on a large scale at a very low cost [15].

3.1.3 Carbon nanocapsules (CNCs)

It has been suggested that carbon-coated magnetic nanoparticles might have important applications in areas such as magnetic data storage, xerography and magnetic resonance imaging. A typical example of carbon nanocapsule is shown in Fig. 3.4. It is a particle containing Fe encapsulated by graphene layers. The role of the carbon layer would be to isolate the particles magnetically from each other, thus avoiding the problems caused by interactions between closely spaced magnetic bits, and to provide oxidation resistance. In addition, the lubricating properties of the graphitic coatings might be helpful in magnetic recording and applications. The potential of important applications has motivated a significant amount of research on the encapsulation of magnetic materials in carbon nanoparticles.

Carbon nanocapsules which there are no metal as core particle can be called as multi-shelled nanoparticles. These particles consist several of graphene sheets in various shapes such as spherical, polyhedral, or short-tube.
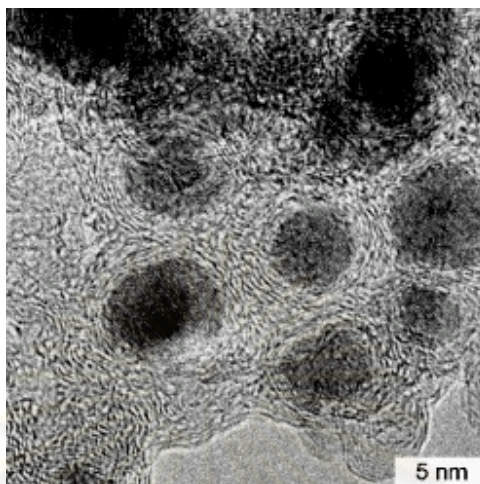
Figure 3.4 Carbon nanocapsules with iron particles in core [10]

3.1.4 Carbon nanohorns (CNHs)

Another type of carbon nanoparticles is named nanohorns due to their irregular horn-like shape, and were discovered by Sumio Iijima's research group. Nanohorns have the same graphitic carbon atom structure as normal carbon nanotubes. The main characteristic of the carbon nanohorns is that when many of the nanohorns group together an aggregate (a secondary particle) of about 100 nanometers is created. The advantage being, that when used as an electrode for a fuel cell, not only is the surface area extremely large, but also, it is easy for the gas and liquid to permeate to the inside. In addition, compared with normal nanotubes, because the nanohorns are easily prepared with high purity it is expected to become a low-cost raw material.
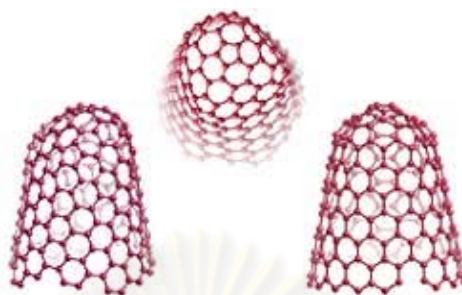
Figure 3.5 Carbon nanohorns (CNHs) model

3.2 Dye

A dye is a colored substance that can be applied in solution or dispersion to a substrate, thus giving a colored appearance. Dye molecules are colored because they are selectively able to absorb and reflect incident light. Organic molecules become colored, and thus useful dye molecules, if they contain at least one of each of the radicals called chromophores and auxochromes.

Chromophores are organic radicals containing unsaturated double bonds. A molecule possessing no chromophores would be colorless. Auxochromes are organic radicals that fulfill the following important functions: intensifies and deeps the hue of the dye molecule's color, makes the dye molecule more readily soluble in water because auxochromes tend to be polar, improves the color fastness properties of the dyed or printed fiber.

3.2.1 Classification of dyes according to application

3.2.1.1 Vat dyes

A vat dye is a water-insoluble colorant containing two or more keto groups. It can thus be brought into aqueous solution by a reduction process (vatting), which converts the vat dye into its alkali-soluble enolic (leuco) form. The major application is the dyeing and printing of cotton. The wash and light fastness of vat dye are excellent. They provide textile materials with the best color fastness of all dyes in common use. Vat dyes have grater exhaustion and fixation than most reactive dyes, and have less color in the effluent. The color removal of vat dyes is much easier owing to its insolubility in water.

3.2.1.2 Sulphur dyes

These dyes are so called because they contain sulphur atoms in their mulecules. These resemble the vat dyes in certain ways. The sulphur dyes contain the characteristic disulphide group in the insoluble form, which can be brought into the aqueous solution by reduction to the alkali-soluble (leuco) form. Sulphur dyes are mainly used for cellulosic fibers and the dyeing is employed for low cost fabrics. The effluent of sulphur dyeing is probably more toxic than any other, due to the presence of sulphide. The wet-fastness of sulphur dyes is usually good and the light-fastness satisfactory, but resistance to bleaching is poor.

3.2.1.3 Reactive dyes

These dyes are characterized by the presence of mobile reactive atoms or groups due to which they may enter into chemical reaction with certain functional group of fibrous materials. They are capable of reacting chemically with a substrate under suitable application conditions to form a covalent dye-substrate bond. The characteristic structural feature is thus the possession of one or more reactive groupings of various kinds. Dyeing with neutral reactive dyes eliminates the need for alkali in fixation and allows complete processing to be performed at a pH of around 7.0. Its application is the dyeing and

printing of cellulosic fibers. Textile materials, which are colored with reactive dyes, have very good wash-fastness and light-fastness, however, they have to be thoroughly rinsed and washed-off to remove the unfixed and the hydrolysed dye molecules. If these molecules of dyes are not removed, poor wet-fastness and rub-fastness may result.

3.2.1.4 Direct dyes

These are defined as anionic dyes with substantivity for cellulosic fibers, normally applied from an aqueous dyebath containing an electrolyte such as sodium chloride. Sodium ions neutralize the negative surface charge of the fiber, enabling the dye anion of direct dye to enter the fiber more readily. The fibers most readily colored with direct dyes are cotton and viscose fibers. At least 70% of direct dyes are unmetallised azo structure. The poor wet-fastness of textile materials dyed with direct dyes are undesirable for many purposes. However, there are many methods to render it less soluble in water and therefore more fast to wet treatment.

3.2.1.5 Disperse dyes

These dyes have affinity for hydrophobic fiber (cellulose acetate) and they are normally applied from fine aqueous dispersion. Hydrophobic fibers can absorb disperse dyes from the vapour phase. This mechanism is the basis of many continuous dyeing and printing methods of application of these dyes. Textile materials which have been dyed with disperse dyes have a fair to good light-fastness and a moderate to good wash-fastness.

3.2.1.6 Basic dyes

Basic dyes are also called cationic dyes because, in solution, the dyes ionize and the colored component always constitutes the cation or positively charge radical. The Society of Dyers and Colorists defines a basic dye as characterized by its substantivity for the acidic types of acrylic fibers and for tannin-mordanted cotton. Acrylic materials dyed and printed with basic dyes have very good light-fastness and wash-fastness. This is

attributed partly to the hydrophobic nature of acrylic fibers, which minimizes their absorption of water and their excellent resistance to sunlight.

3.2.1.7 Acid dyes

The acid dyes are so called because the original members of the class were applied under acidic conditions, and they are nearly all sodium salts of organic acids and the anion is the active colored component. These are defined as anionic dyes, characterized by substantivity for protein fibers. Wood, silk and nylon contain basic groups and the uptake of leveling acid dyes by nylon at acidic pH can usually be relate to the amine end-group content of fiber. As well as the dyeing and printing of nylon and protein fibers, acid dyes are important for the coloration of leather, paper, jute, wool and anodised aluminium. Metal toners are concentrated pigments prepared by precipitating anionic dyes, often of the unmetallised azo acid type, as their water-insoluble metal salts. Dyes and printed acid colors have good light-fastness.

3.2.1.8 Mordant dyes

The somewhat ambiguous term 'mordant dye' is defined as a dye that is fixed with a 'mordant'. A mordant is itself defined as 'a substance, usually a metallic compound, applied to a substrate to form a complex with a dye, which is retained by the substrate more firmly than the dye itself'. A more logical generic name for those chelatable anionic dyes capable of being fixed to wool after treatment with a dichromate would be the more popular term 'chrome dye' or 'chrome mordant dyes'.

3.2.1.9 Solvent dyes

Solvent dyes are characterized by their solubility in one or more organic solvents. Numerous media of interest in practice are alcohols, ethers, esters, ketones, chlorinated solvents, hydrocarbons, oils, fats and waxes.

3.2.2 Textile wastewater treatment methods

Textile processing includes sizing, desizing, scouring, bleaching, mercerization, weaving, dyeing, printing and finishing. The dyeing operation involves the use of chemicals, such as salt, alkalis, acids, reducing agents, oxidizing gents, soaps and detergents, and dye-fixing agents. Textile wastewater is generally colored, highly alkaline, highly in BOD or COD values, and high in suspended solids. One of the major problems concerning textile wastewaters is colored effluent. Though not particularly toxic, dyes have a visible effect. The presence of color will reduce aquatic diversity by blocking the passage of light through the water. There are many methods which have been applied for removed the color from wastewater such as coagulation, chemical flocculation, biological treatment, chemical oxidation, chemical reduction and adsorption.

One possible treatment for the removal of soluble dyes by an aerobic procedure may be biodegradation, but reactive dyes constitute an exception. The effluents containing azo reactive dyes are very difficult to treat in environmental systems, due to its high water soluble and polar.

Adsorption is one of the most effective physical processes for the removal of color and treatment of textile effluents. In the adsorption procedures the conventional materials used is activated carbon, but due to its complicacy in operation and separation. Then the alternative carbon material adsorbents, which are easier than in its operation and separation, have been studies.

3.3 Adsorption

When two phases are in contact, there is a region at their interface the composition of which is different from that of the bulk of either phase. The increase in the concentration of a substance at the interface as compared with the bulk concentration, is known as adsorption. On the surface of solid, substance can be adsorbed from a gaseous or liquid phase. The solid is known as the adsorbent and the gas or liquid is called the adsorbate.

Adsorption is brought about by the interactions between the solid and the molecules in the fluid phase.
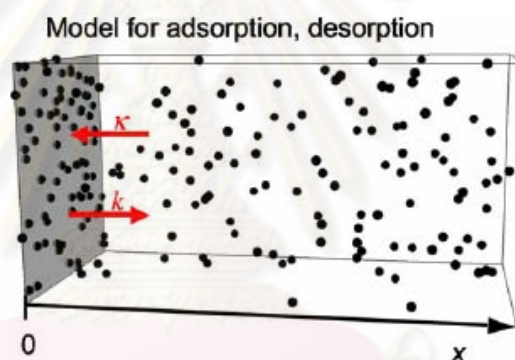
Figure 3.6 Model system for adsorption and desorption.

Figure 3.6 presents model for adsorption and desorption where molecules shown with dots, adsorb to the gray surface with the adsorption coefficient (K) and desorb with the rate constant (k'). Equilibrium would take place once the system is kept under a condition of constant temperature and pressure with the presence of sufficient amount of adsorbate molecules. Adsorption equilibrium would be affected by the adsorption capacity of the adsorbing surface and intensive properties of adsorbed molecules.

3.3.1 Types of adsorption

3.3.1.1 Physical adsorption, or Physisorption

It is relative nonspecific and is due to the operation of weak forces of attraction or van der Waals's forces between molecules. Here, the adsorbed molecule is not affixed to a particular site on the solid surface, but it free to move about over the surface because the surface does not share electrons with the adsorbate. When the molecular forces of attraction between the adsorbate and the adsorbent are greater than the forces of attraction between the adsorbate and the solvent, the adsorbate will be adsorbed onto the adsorbent surface. The adsorbent has numerous capillaries within the particles, and the surface available for adsorption includes the surface of the pores in addition to the external surface of the particle. Actually, most of the adsorption occurs on the pore surfaces. In addition, the adsorbed material may condense and form several superimposed layers on the surface of the adsorbent. Physical adsorption is generally quite reversible. Physisorption has a comparatively low enthalpy of adsorption, typically are only 2-20 kcal/mole.

3.3.1.2 Chemical adsorption, or Chemisorption

It is associated with exchange of electrons and the formation of a chemical bond between the adsorbed molecule (adsorbate) and the surface (adsorbent), which results in much stronger forces. Normally the adsorbed material forms a layer over the surface which is only one molecule thick, and the molecules are not considered free to move from one surface site to another. When the surface is cover by the monomolecular layer, the capacity of the adsorbent is essentially exhausted. Also, chemical adsorption is seldom reversible. Eckenfelder (2000) explained that the chemical adsorption results in the formation of a monomolecular layer of the adsorbate on the surface through forces of residual valence of the surface molecule [25]. A wide range of enthalpy changes may occur on chemisorption, though the typical chemisorption energies are 15-100 kcal/mole for simple molecules.

Therefore, a molecule is chemisorbed if the molecule's electronic structure is significantly perturbed upon adsorption, while a molecule is physisorbed if it adsorbs without undergoing a significant change in electronic structure. Molecules are often distorted when they adsorb on solid surfaces. Sometimes the molecules stay intact during the adsorption process, while at other times the bond break. A molecule can usually be physisorbed and chemisorbed on the same surface. The process may often be explained by an electrical attraction to the solid phase of components with a (minor) electrical change. The adsorption results in the formation of a molecular layer of the adsorbate on the surface and is sometimes followed by a slow diffusion into the particles of the adsorbent.

3.3.2 Adsorption isotherm

When an adsorbent is placed in a solution containing an organic solute and the slurry is agitated or mixed to give adequate contact, adsorption of the solute occurs. The solute concentration will decrease from an initial concentration, C_0, to an equilibrium value, C_e, if the contact time is sufficient during the slurry test. Adsorption isotherm is the relation between amount of solute adsorbed per unit mass of adsorbent (Q_e) and the equilibrium concentration (C_e) at a constant temperature. The isotherm can be graphically reduced to a straight line, for example, for the Langmuir equation and for the Freundlich equation. Thus correlation of equilibrium data by either theoretical or empirical equations is essential to practical operation. Two famous adsorption isotherm models have been proposed as follows.

3.3.2.1 Langmuir isotherm

In 1918, Irving Langmuir proposed another adsorption isotherm which explained the variation of Adsorption. It is an empirical isotherm derived from a proposed kinetic mechanism [32]. It is based on four hypotheses:

- The surface of the adsorbent is uniform, that is, all the adsorption sites are equal.
- Adsorbed molecules do not interact.
- All adsorption occurs through the same mechanism.
- At the maximum adsorption, only a monolayer is formed: molecules of adsorbate do not deposit on other, already adsorbed, molecules of adsorbate, only on the free surface of the adsorbent.

The theoretical Langmuir isotherm is valid for adsorption of a solute from a liquid solution as monolayer adsorption on a surface containing a finite number of identical sites. Langmuir isotherm model assumes uniform energies of adsorption onto the surface without transmigration of adsorbate in the plane of the surface. The Langmuir equation is the most widely used parameter equation, as Eq. 3.1.

Langmuir equation:
$$\frac{C_e}{Q_e} = \frac{C_e}{Q_m} + \frac{1}{K_L Q_m} \qquad (3.1)$$

and
$$R_L = \frac{1}{1 + K_L C_0} \qquad (3.2)$$

where C_e (mg/L) is the concentration of dye at equilibrium, Q_e (mg/g) is the amount of dye adsorbed at equilibrium, Q_m (mg/g) is the maximum adsorption capacity and K_L (L/mg) is the Langmuir constant. The values of Q_m and K_L can be calculated from plotting C_e/Q_e versus C_e.

The maximum adsorption capacity is corresponding to monolayer coverage.
From Eq. 3.2, the separation factor or equilibrium parameter (R_L) also evaluated.

(i) $R_L = 0$: The adsorption process is irreversible
(ii) $R_L = 1$: Linear adsorption
(iii) $R_L > 1$: Unfavorable adsorption
(iv) $0 < R_L < 1$: Favorable adsorption

3.3.2.2 Freundlich isotherm

The Freundlich isotherm model assumes heterogeneous surface energies, in which the energy term in the Langmuir equation varies as a function of the surface coverage. It is the most important multisite adsorption isotherm for rough surface.

The Freundlich isotherm model is the earliest known equation describing the adsorption process. It is an empirical equation and can be used for non-ideal sorption that involves heterogeneous adsorption. The empirical Freundlich equation is given below by Eq. 3.3 or 3.4.

Freundlich equation: $\quad Q_e = K_F C_e^{1/n}$ \hfill (3.3)

$$\log Q_e = \log K_F + \frac{1}{n} \log C_e \qquad (3.4)$$

where Qe (mg/g) is the amount of dye adsorbed at equilibrium, Ce (mg/L) is the concentration of dye in solution at equilibrium, K_F (mg/g (mg/L)$^{1/n}$) and 1/n are Freundlich constants related to adsorption capacity and adsorption intensity, respectively.

The magnitude of $1/n$ quantifies the favorability of adsorption and the degree of heterogeneity of the CNTs surface. If $1/n$ is less than unity, indicating favorable adsorption and the adsorption is physical, then the adsorption capacity increases and new adsorption sites occur. Otherwise, the adsorption is chemical.

CHAPTER IV
EXPERIMENTAL

Procedures of experiment and analysis techniques are described in this chapter. This research emphasizes on removal of dye in aqueous solutions with CNPs adsorbent as a batch operation which are explained in 4.3 and 4.4. The analysis instruments necessary for characterization all relevant substance and methods are also shown in 4.5.

Before adsorption experiment, synthesizing of CNPs with magnetic characteristics are conducted with available equipment. The experimental apparatus for synthesizing CNPs are represented in 4.1 and the experimental procedures for synthesizing CNPs are also described in 4.2 as follows.

4.1 Experimental setup for synthesizing of CNPs

The preliminary part of this work is to use a tubular quartz reactor for synthesizing of carbon nanoparticles. There are many researches which use a similar reactor with single and dual tube furnace reactor for pyrolysis of various carbon sources. For this work, a single tube furnace reactor is applied from Charinpanitkul's research [7]. The advantage of the single tube furnace is the continuity of temperature profile in the tube is better than that of the dual furnace although it has a problem in controlling the vaporization temperature of the raw materials used in the process. The schematic diagram of experimental apparatus has shown in Figure 4.1.
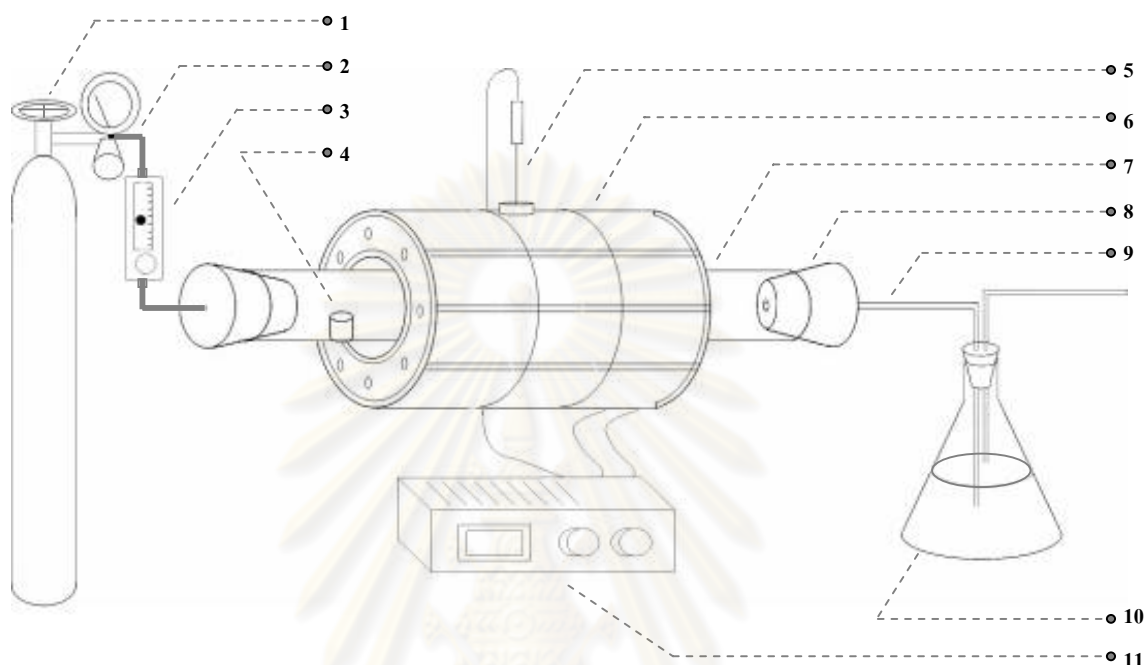
Figure 4.1 Schematic diagrams of experimental apparatus for thermal co-pyrolysis

1) Nitrogen storage tank   2) Regulator   3) Flow meter   4) Ceramic boat

5) Thermocouple   6) Electrical furnace   7) Tubular quartz reactor 8) Silicone plugs

9) Rubber tube   10) Water trapping   11) Temperature controller

It is consisted of tube furnace reactor (Figure 4.2) equipped with temperature controller (Figure 4.3) for controlling the pyrolysis temperature at 900 ˚C. Quartz tube with 4.1 cm inner diameter and 60 cm length (Figure 4.4) is used for co-pyrolyzing the mixture of precursors. The gas supplier will provide carrier gas during the pyrolysis process and silicone plug (Figure 4.5) has been used for preventing the process from other gas. The gas from the process will be removed by trapping with water before purging to outside.

Figure 4.2 Electrical furnace

Figure 4.3 Temperature controller

Figure 4.4 Quartz tube with inner diameter of 41 mm.

Figure 4.5 Silicone Plug for controlling leakage of gas

Figure 4.6 Ceramic boat for situating raw materials

4.2 Experimental procedures for synthesizing CNPs by co-pyrolysis

The tubular quartz reactor set within the temperature controlled furnace shown in figure 4.1 is employed for co-pyrolyzing mixture of ferrocene and glycerol to synthesize carbon nanoparticles. The apparatus consists of a single-stage furnace equipped with temperature controller and quartz tube (inner diameter, 41 mm). The nitrogen gas (nitrogen 99.99%) which used as carrier gas is fed continuously through a flow meter at desired flow rate. The experimental procedures are shown as follows;

a) The furnace temperature will be set a designated set point of 900 °C by using temperature controller.

b) Ferrocene (Sigma-Aldrich, ≥98% Fe, b.p. = 249 ℃) and glycerol (Ajax Chemicals, b.p. = 290 ℃) are mixed to adjust a specific molar ratio of 1:5 of ferrocene to glycerol and then are loaded into a ceramic boat (Figure 4.6) which is placed at the entrance of the quartz tube reactor where the temperature is kept above the vaporization temperature of the mixture.

c) The decomposition of the mixture occurred at about 400℃, resulting in free carbon and iron vapor which are carried over by the carrier gas at 100 ml/min through the tube into the hot zone where self-assembling and catalytic growth reactions took place.

d) Large quantities of the as-grown deposit films as in Figure 4.6 can be found as accumulation along the inner surface of the quartz tube after reaction complete (30 min). The detailed experimental parameters are represented in Table 4.1.

Table 4.1 The condition for co-pyrolysis work studied

F^a:G^b molar ratio	1:5
Amount of F/G (g)	2.3022/0.9300
Amount of Fe/C (g)	55.845/636.5671
Carrier gas	N_2
Operation temperature ($^\circ$C)	900

^{a}Ferrocene, ^{b}Glycerol

Figure 4.7 As-grown carbon nanoparticles obtained from co-pyrolysis process

ศูนย์วิทยทรัพยากร

จุฬาลงกรณ์มหาวิทยาลัย

4.3 Experimental setup for dye pollutant removal

4.3.1 Preparation of dye solution

Synthetic dye solution of B5, R31 and MB are prepared by dissolving the dyes powder in distilled water at desire initial concentration. The model structure of all dyes in this study is shown in figure 4.8. The wavelength of maximum absorbance (λ_{max}) was analyzed with a spectrophotometer by scanning in the visible range of 400 to 800 nm, as shown in Table 4.2.

Table 4.2 Properties of dyes in this study

Name in Color Index	Commercial Name	MW.	λ_{max} (nm)	Molecular Formular
C.I. Reactive Black 5 (B5)	Benefix Black B	991.82	595	$C_{26}H_{21}N_5O_{19}Na_4S_6$
C.I. Reactive Red 31 (R31)	Benecion Red P8B	864	545	$C_{30}H_{15}N_7O_{15}Na_5Cl$
C.I. Basic Blue 9 (MB)	Methylene Blue	319.85	664	$C_{16}H_{18}N_3SCl$
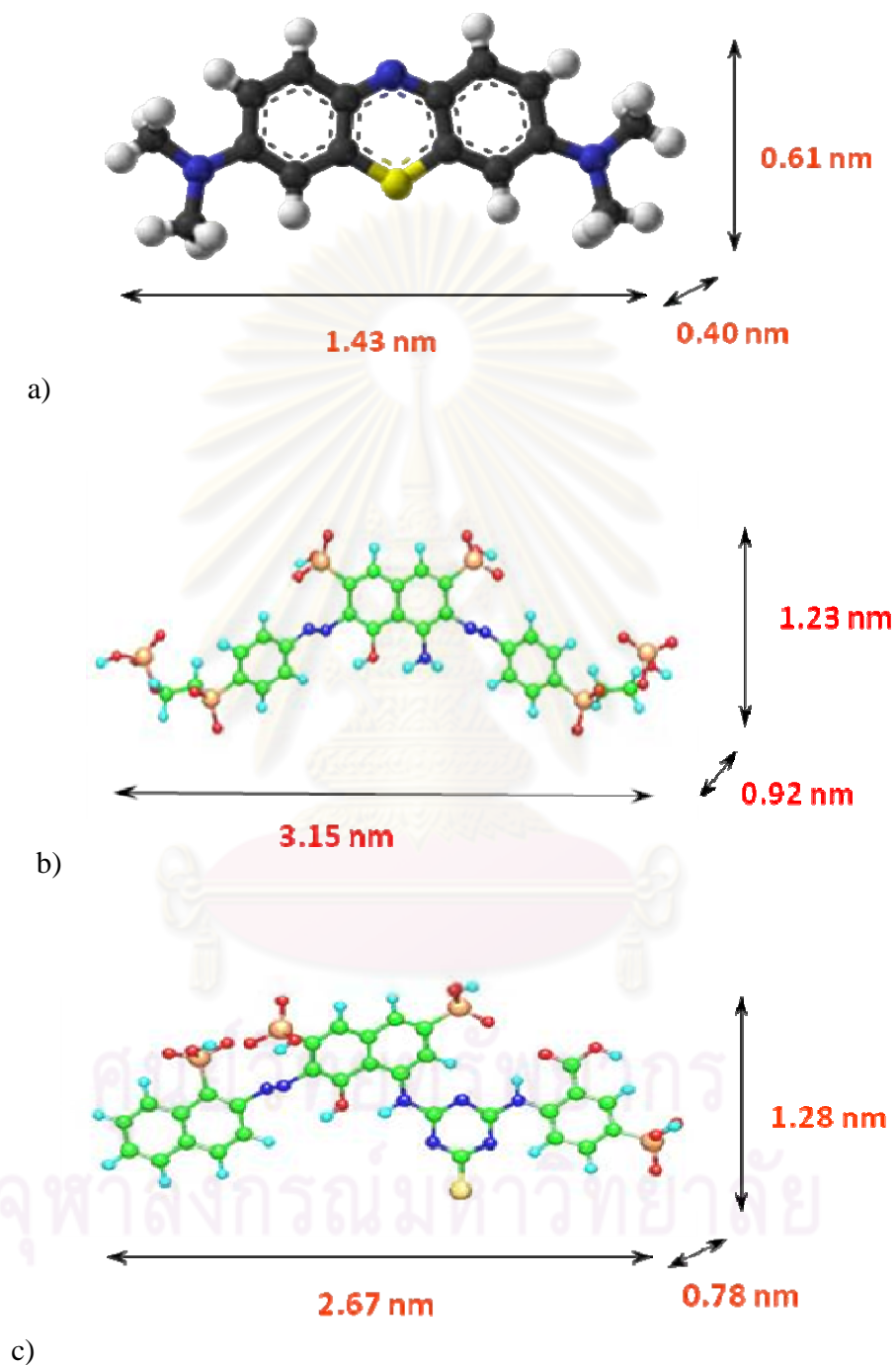
Figure 4.8 Molecular model of adsorbates: a) Methylene Blue, b) Reactive Black 5 and
c) Reactive Red 31

4.3.2 Batch experimental

Batch system is used in sorption experiment with a shaker bath as shown in figure 4.9. All batch experiments are conducted at designated initial dye concentration, pH solution and dose of adsorbents by shaking 100 ml dye solution in 250-ml flask, using a speed of 100 rpm with a temperature of $25 \pm 2°C$ in water tank.
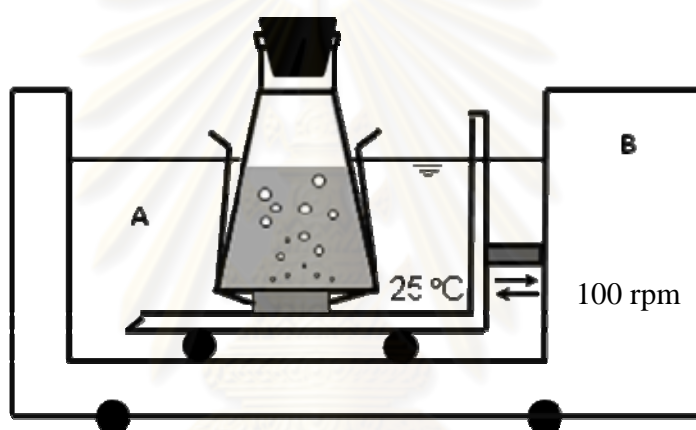
Figure 4.9 Schematic diagram of batch system for adsorption experiment
(A) dye solution in 250-ml flask; (B) horizontal shaker bath with
controlled temperature of 25 °C.

4.4 Experimental procedures for dye sorption onto synthesized CNPs

The adsorption and desorption of the synthetic dye on synthesized MWCNTs are investigated. All experiments are conducted in batch system. The experimental are carried out in 250 ml glass bottle at $25 \pm 2°C$, and 100 ml of dye solution of known initial concentration which are prepared in distilled water. NaOH and HCl 0.01 mM are used to adjust the initial pH value of solution. CNPs as adsorbent are added into glass bottle with desired quantity. Then, CNPs are dispersed in solution with ultrasonic for 10 minutes and shaking by shaker bath at a speed of 100 rpm. The concentration of dyes in effluent solution is measured by UV-visible spectrophotometer (UV-1700PC, Shimadzu, Japan). Three repeated experiments were conducted, leading to a summarized result. Table 4.3 showed variables of this study. The adsorption procedures are described below.

a) Condition of contact time study is the initial dye concentration of 40 mg/L, 0.5 g/L adsorbent and initial pH value of 6. Take sample until the adsorption reach equilibrium to determine the minimum time require.

b) Effect of the initial dye concentration is investigated to determine the maximum adsorption capacity and compare with the adsorption isotherm model. The experiments are performed in the range of 10 to 100 mg/L, 300 minutes of contact time, 0.5 g/L adsorbent and initial pH value of 6.

c) Effect of CNPs loading are performed in the range of 0.3 to 0.9 g/L, initial concentration of 60 mg/L, 300 minutes of contact time and initial pH value of 6.

d) Effect of initial pH value is performed in the range of 3 to 11.

Table 4.3 Variables of the adsorption experiments.

Study	Variables			
	Initial dye concentration (mg/L)	Initial pH value	Dose of adsorbents (g/L)	Temp. and Contact time (°C and min)
Effect of contact time	40	6	0.5	25 ± 2, 300
Effect of initial dye concentration	10 - 100	6	0.5	25 ± 2, 300
Effect of CNPs loading	60	6	0.3 - 0.9	25 ± 2, 300
Effect of initial pH values	100	3 - 11	0.5	25 ± 2, 300

The condition of desorption experiment are initial dye concentration of 100 mg/l, 0.5 g/L adsorbent and 24 hours of adsorption time at 25 °C and the initial pH value of 6. After adsorption, adsorbents were seperated from the solution by an external permanent magnetic and oven-dried at 80 °C to a constant mass. The solution was measured the concentration with UV-spectrophotometer.

Exhausted CNPs were suspended in distillated water which was adjusted the pH value. In this study, the range of initial pH value of the solution is 3-11. Re-adsorption experiment following the procedure described above for 3 cycles.

4.5   Analytical Instruments

The morphology of the as-grown samples was first analyzed by Scanning electron microscope (SEM, JEOL: JSM-5410LV, Japan). The structure and crystallinity of the as-grown samples were investigated by Transmission Electron Microscope (TEM, JEOL: JEOL-2010, Japan). The crystallinity of CNPs was evaluated by X-ray Diffraction analysis. While dynamic light scattering (DLS; MALVERN, ZETASIZER 300HSA) is employed for determining particles size distribution and zeta potential of the obtained products.

4.5.1 Scanning Electron Microscopy (SEM)

The microstructure of the carbon nanoparticles were studied by using Scanning Electron Microscopy (SEM), JSM-5410LV (Figure 4.10). The specimen used for SEM analysis was either obtained from the as-grown film or scratched (Figure 4.7). The sample was prepared by grinding using a granite mortar and then appropriate amount of the prepared samples were mounted on carbon tape. The specimens were loaded into the sample chamber and then the observation was conducted immediately with using image catcher scanner for taking the photos.

Figure 4.10 Scanning Electron Microscope (SEM, JEOL: JSM-5410LV, Japan)

4.5.2 Energy Dispersive X-ray Spectroscopy (EDX)

Energy dispersive X-ray spectroscopy is a relatively simple technique used to identify the elemental composition of a cubic micron of material. The equipment is attached to the SEM to allow for elemental information to be gathered about the specimen under investigation. The technique is non-destructive and has a sensitivity of >0.1% for elements heavier than C.

EDX works by detecting X-rays that are produced by a sample placed in an electron beam. The electron beam excites the atoms in the sample that subsequently produce X-rays to discharge the excess energy. The energy of the X-rays is characteristic of the atoms that produced them, forming peaks in the spectrum. The individual elements may have more than one peak associated with them and some peaks from different elements may overlap to a certain degree.

The samples were analyzed by energy-dispersive X-ray spectra (EDX) to show elemental component in the obtained particles after co-pyrolysis process. The elemental analysis by EDX is achieved by monitoring and analyzing X-rays emitted by matter when bombarded with charged particles. The JEOL JSM-5410LV SEM is equipped with an Oxford Link Isis - Energy Dispersive X-ray Spectrometer (EDX), which serves as an elemental analyzer. The solid state Si(Li) detector, permits the detection of X-rays and identification of the elements responsible for the emission in a microscopic location.

4.5.2 Transmission Electron Microscopy (TEM)

TEM analysis used in this work is JEOL-2010 as shown in Figure 4.11. The specimen for analyzing was elaborately prepared by grinding as-grown particles deposit (Figure 4.7) by a granite mortar. The appropriate amounts of carbon nanoparticles were suspended in toluene before ultrasonic treatment with the sufficient time for ensuring its uniform dispersion. A few drop of clear solution was poured onto a microgrid covered with a carbon thin film (Figure 4.12). The specimen was loaded into the sample chamber and waiting for the vaccum condition and steady state inside the chamber for 30 min.

Figure 4.11 Transmission Electron Microscopy (TEM JEOL: JEOL-2010, Japan)

Figure 4.12 Copper grid coated with carbon films for

Transmission Electron Microscopy

4.5.3 Dynamic Light Scattering (DLS)

For particle size distribution analysis, Dynamic Light Scattering (DLS) using ZETASIZER 300HSA as shown in Figure 4.13 was employed. It should be noted that DLS is based on the measurement of the dispersion of light scattering by particles motion in a static solvent such as toluene, water, acetone or ethanol, the measured particle size should correspond to hydrodynamic diameter but not to the real diameters of the particles with complex structures. However, DLS results were expected to give at least the qualitative trend in particle sizes distribution. Moreover, zeta potential of sample can be obtained by this measurement. For preparation of the sample, DLS specimens were also prepared by grinding as-grown particles (Figure 4.7) by the granite mortar and then suspended in toluene before ultrasonic treatment with the sufficient time for ensuring its uniform dispersion. Afterwards, the specimen was diluted by toluene again until they became transparent and ultrasonicated again for 15 min before loading to the sample cell for analysis.

Figure 4.13 Dynamic Light Scattering (DLS: ZETASIZER 300HSA)

4.5.4 Porosity analysis

Porous structure of the obtained CNPs (see figure 4.7) by co-pyrolysis process was characterized by nitrogen adsorption – desorption at 77 K with a BET analyzer (*BEL: BELSORP-mini, Japan*) as shown in Figure 4.14. The CNPs sample about 0.8 grams was pretreated at 150°C under vacuum for 3 hours in order to remove moisture and gaseous residual. Brunauer–Emmett–Teller (BET) surface area (S_{BET}) and total pore volume (V_{tot}) were determined by BET equation and mesopore volume (V_{mes}) was determined by BJH (Barrett-Joyner-Halenda) plot method. Moreover, average pore diameter of synthesized CNPs was also determined.

Figure 4.14 N_2 adsorption – desorption analyzer (*BEL: BELSORP-mini, Japan*)

4.5.5 X-ray diffraction (XRD)

Structure and crystallinity of CNPs particles was determined by X-ray diffraction analysis. The as-grown CNPs samples (see Figure 4.7) were characterized by X-ray powder diffraction (*XRD, SIEMENS D 5000, Japan*) as shown in Figure 4.15 using CuKα radiation with Ni filter in the 2q range of 20-80 degrees resolution 0.04°. The crystallite size was calculated from Scherrer's equation.

Figure 4.15 X-ray diffraction analyzer (*XRD, SIEMENS D 5000, Japan*)

4.5.6 UV-Visible spectrophotometer

For measure the concentration change, Ultraviolet and visible spectrophotometer as shown in figure 4.16 was employed. The UV-Visible spectrophotometer uses two light sources, a deuterium (D_2) lamp for ultraviolet light and a tungsten (W) lamp for visible light. After bouncing off a mirror, the light beam passes through a slit and hits a diffraction grating. The grating can be rotated allowing for a specific wavelength to be selected. At any specific orientation of the grating, only single wavelength successfully passes through a slit. A filter is used to remove unwanted higher orders of diffraction. The light beam hits a second mirror before it gets split by a half mirror (half of the light is reflected, the other half passes through). One of the beams is allowed to pass through a reference cuvette (which contains the solvent only), the other passes through the sample cuvette. The intensities of the light beams are then measured at the end.

Figure 4.16 UV-vis spectrophotometer (Shimatsu: UV-1700PC, Japan)

CHAPTER V

RESULTS AND DISCUSSION

5.1 Synthesis of Carbon nanoparticles

5.1.1 Temperature profile of the tubular quartz reactor

Since a tubular reactor is employed for pyrolysis of ferrocene and glycerol mixture the temperature distribution along the axial direction of the reactor is a crucial parameter to be known before conducting other experiments. The temperature profile has been determined by inserting the thermocouple into the tube then moving its tip with a step size of 2 centimeters after achieving the set point of 900 °C. The temperature distribution has been shown in figure 5.1. The curve exhibits a symmetric distribution and a maximum value is at the middle of the tube. In practice, the mixture of ferrocene and glycerol contained in an alumina boat was placed at the position of which temperature is higher than $300^{°}C$ (14 cm. from inlet) in the experiment because it is the condition that the mixture could be vaporized without decomposition.

Pyrolysis process has been started by vaporization of the mixture and nitrogen gas as a carrier gas will carry the vapors to the downstream zone where the decomposition could take place. After the operating time of 30 minutes, the obtained product is collected by sweeping from the inner tube wall. The products have been characterized by electron microscopy, EDX, XRD, DLS with zeta potential analysis and BET analysis.
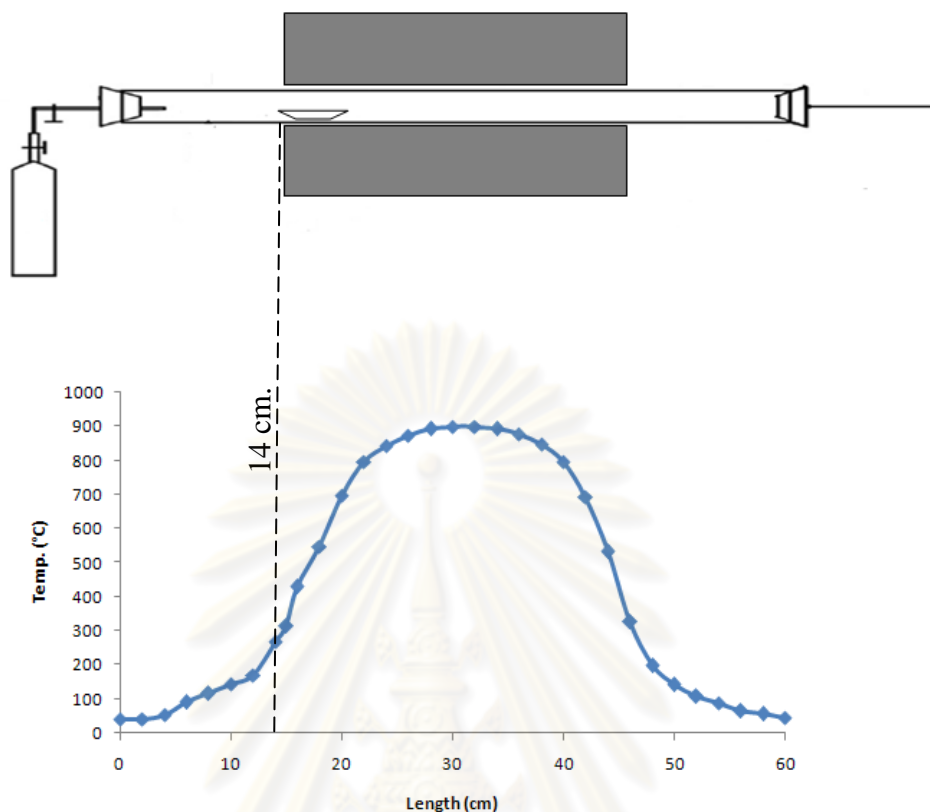
Figure 5.1 Temperature distribution of the reactor

5.1.2 Microscopic analysis

5.1.2.1 SEM and TEM analysis

As the product from co-pyrolysis process, a black film fully coved the inner surface of the tubular quartz reactor wall. The synthesized products were swept from the inner wall surface for SEM and TEM analysis.

Bases on typical SEM observation, the as-grown product consists of large amount of entangling carbon nanotubes (CNTs) with a few spherical carbon nanoparticles as shown in figure 5.2. The obtained product is CNTs with diameters of 40 to 80 nm with length of several microns. However, some agglomerations of very fine particles also deposit on the tube tube bundle surface. On the top edge of the tube bundles, there are many fine particles with different morphology as shown in figure 5.3. It would be able to verify later that those particles are iron clusters encapsulated in carbon shell.
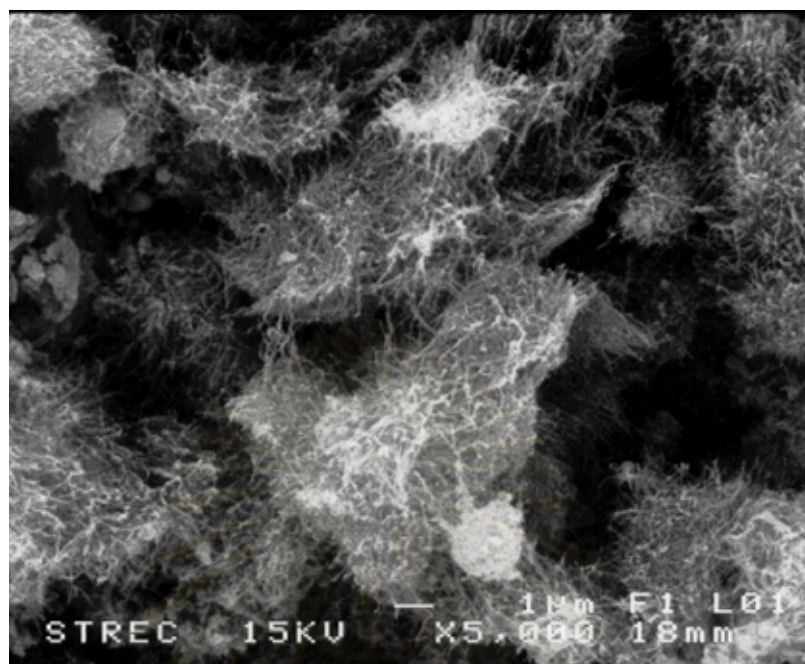
Figure 5.2 SEM images of the synthesized products
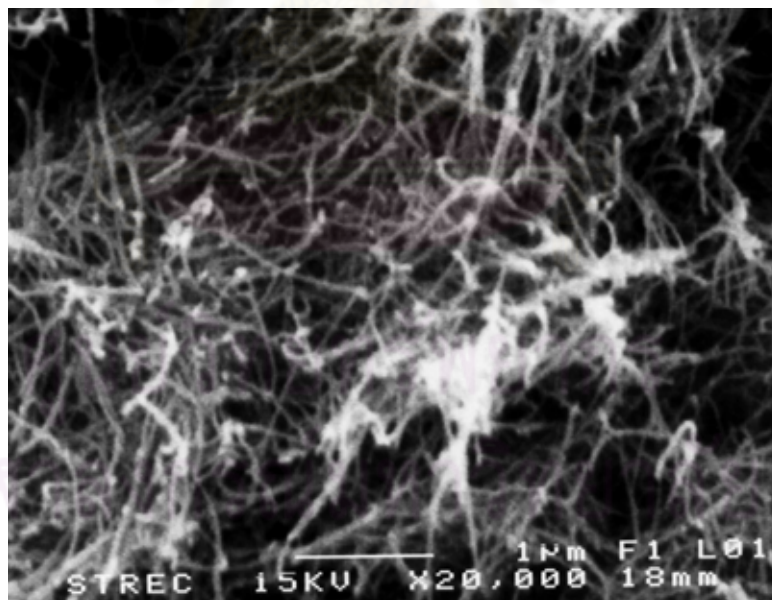
Figure 5.3 Higher magnification of SEM images of the synthesized products

For further investigation of the morphology of the synthesized products, a carefully sampled product is dispersed in toluene and ultrasonicated before dropped on a copper grid for TEM observation. As shown in figure 5.4, the low magnification of the TEM image of the obtained product illustrates that most of the obtained particles are CNTs with diameters of 40-80 nm and carbon nanocapsules (CNCs). Moreover, the obtained products are multi-walled carbon nanotubes (MWCNTs) with iron particles filled in the tubes and at the tube tip and multi-shell carbon nanocapsules with iron particles which were encapsulated in the core. These results are in good agreement with the SEM observation that the as-grown product consists of large amount of entangling carbon nanotubes.
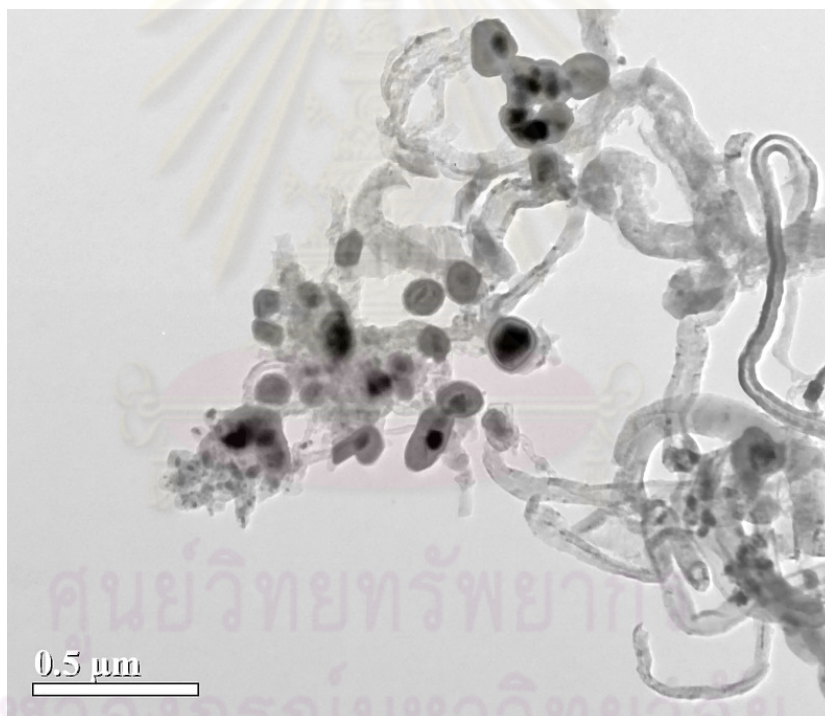
Figure 5.4 The low magnification of the TEM image

Higher magnification of TEM images of CNPs obtained also reveals that the obtained nanotubes are multi-walled carbon nanotubes (MWCNTs) and the obtained spherical carbon nanoparticles are multi-shell carbon nanocapsules as shown in figure 5.5. It suggests that these products are obtained from the growth of carbon atoms induced by iron clusters. As also prepared by Charinpanitkul et al. (2009) and Sano et al. (2004), formation of carbon shell would take place after the condensation of Fe clusters emitted from the decomposition of ferrocene [2, 7]. Because of the presence of Fe clusters within the internal structure of these carbon nanoparticles, our synthesized products exhibit a good respond to magnetic field.
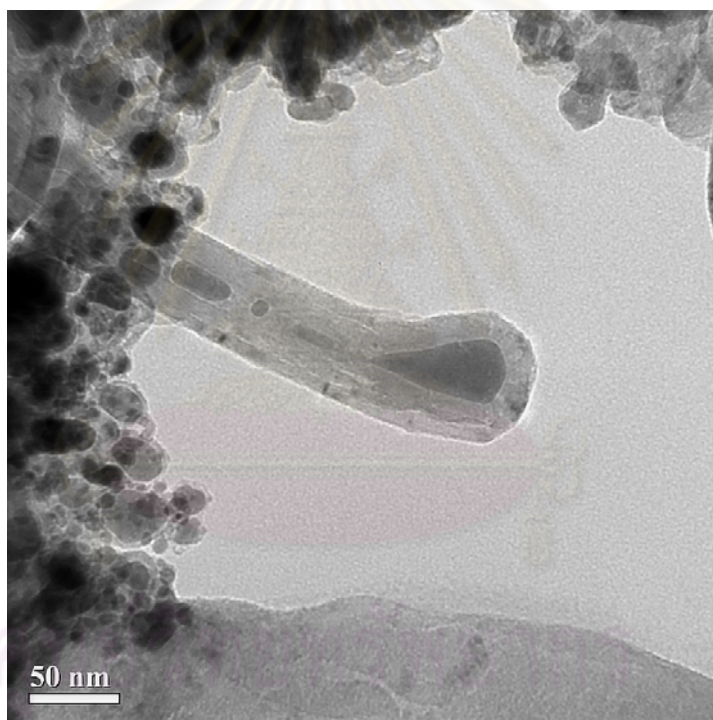
Figure 5.5 Higher magnification of the TEM image

5.1.2.2 Elemental analysis

5.1.2.2.1 Energy dispersive X-ray (EDX)

The energy dispersive X-ray (EDX) spectroscopic analysis has been performed for elemental analysis as shown in figure 5.6. From the result, it is found that the obtained products were composed mainly of carbon (77.34 wt %) and Fe (14.32 wt %). This confirms that iron particles exist in the synthesized products. Further investigation on the phase and crystalline structure of these Fe clusters would be conducted by XRD analyzer and discussed later in 5.1.2.2.2.
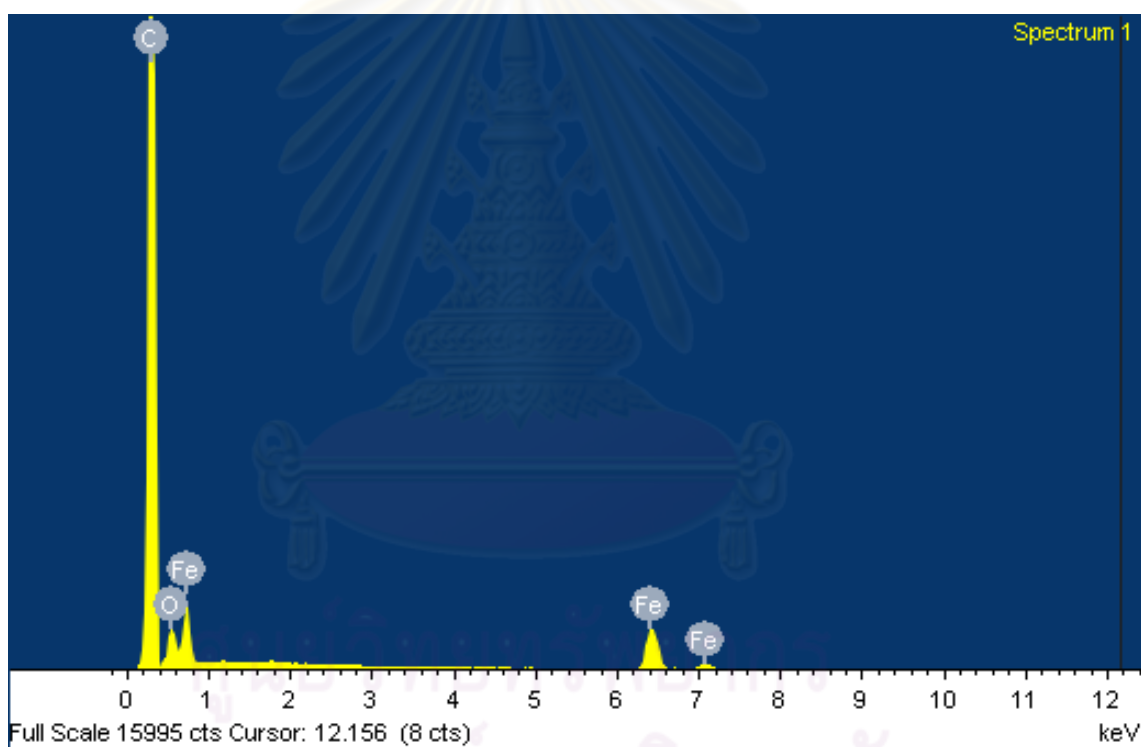
Figure 5.6 EDX spectrum of CNTs from co-pyrolysis at 900 °C

5.1.2.2.2 X-ray Diffraction (XRD) analysis

XRD characterization is performed to further validate the corresponding structure of the core and shell of nanoparticles. The XRD result of the as-synthesized products from ferrocene-glycerol mixture with molar ratio of 5:1 at 900°C is shown in figure 5.7. The diffraction peak at about 26.3° can be assigned to the (002) planes of hexagonal graphite structure. The iron cores are crystalline and exhibit the (110) plane of the fcc-Fe crystal (face-centered cubic) at XRD peak 43.7°. In addition, it can be seen the others peak from the result such as: bcc-Fe (110) at 44.7°, fcc-Fe (200) at 48.8°. However, it can observe iron carbide (Fe_3C) and iron oxide (Fe_2O_3) with including in the as-grown prepared CNPs.
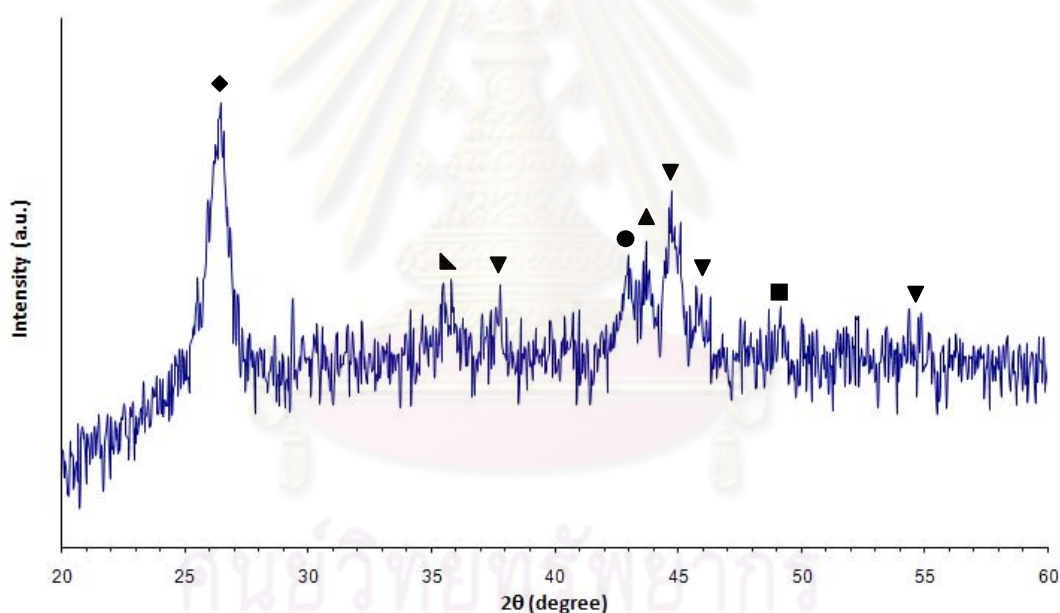
Figure 5.7 XRD pattern of products obtained at 900° C with molar ratio of 1:5

♦ (002) Graphite structure (26.3°)   ▲ (110) bcc-Fe (44.7°)

● (111) fcc Fe (43.7°)   ▼ Fe_3C (iron carbide)

■ (200) fcc-Fe (48.8°)   ◣ Fe_2O_3

It should be noted that the iron particles in the as-grown products are in the form of iron oxide (Fe_2O_3), which is obtained by a reaction of oxygen remained in the process from glycerol, and in the phase of iron carbide (Fe_3C) and metallic phase of bcc-Fe (110) fcc-Fe (111) and fcc-Fe (200). The well-crystallized graphite could be recognized as higher diffraction peak.

5.1.2.2.3 Dynamic Light Scattering (DLS) with zeta potential

Dynamic Light Scattering characterization is performed to determining particle size distribution and zeta potential of the synthesized CNPs. The as-grown film of CNPs is sampled and dispersed in toluene and then ultrasonicated for 15 minutes. A typical well dispersed sample is characterized for their particle size distribution by ZETASIZER 300HSA as which is shown in figure 5.8.

Based on experimental results, the hydrodynamic diameter of the obtained CNPs is in a range of 105-1200 nm which higher than SEM observation due to the agglomeration of the obtained CNPs.

Figure 5.8 Particle size distributions of CNPs obtained from co-pyrolysis of Ferrocene and Glycerol with molar ratio of 1: 5 at 900 °C.
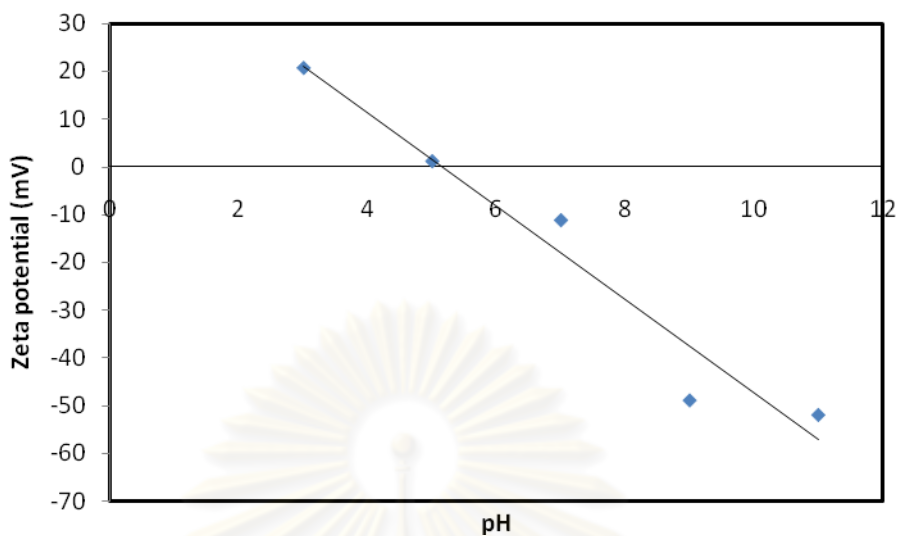
Figure 5.9 zeta potential of the CNPs.

The as-grown CNPs is also characterized for zeta potential as shown in figure 5.9. From the zeta potential result, it is indicated that the surface of CNPs was positively charged when solution pH was below 5.1 and negatively charge when solution pH was above 5.1. Therefore, it should be note that the pH of the zero point of charge (pH_{zpc}) for the obtained CNPs was determined to be 5.1 which similar with the results of Wu [17] and Kuo et al. [18].

5.1.3 Porosity analysis

The porosity of synthesized CNPs was determined by adsorption-desorption of nitrogen gas at 77 K using a BET analyzer (*BEL: BELSORP-mini, Japan*). Typical isotherms of adsorption-desorption of synthesized CNPs was demonstrated in Figure 5.10. From the result, the isotherm of synthesized CNPs can be classified as a type IV isotherm, according to the International Union of Pure and Applied Chemistry (IUPAC) nomenclature [23] which indicated the existence of micropore and mesopore structure. Specific BET surface area (S_{BET}), total pore volume (V_{tot}), mesopore volume (V_{mes}) and average pore diameter (D_{avg}) are presented in table 5.1. The pore size distribution data calculated (as shown in figure 5.11) from the adsorption branches of nitrogen isotherms by the BJH (Barrett-Joyner-Halenda) method showed that the synthesized CNPs exhibit a modal pore size radius of 3.76 nm with a noticeable pore size radius distribution smaller than 100 nm.

Table 5.1 Porosity analysis of synthesized CNPs

N$_2$ adsorption-desorption at 77 K	
S_{BET} [m^2/g]	73.851
V_{tot} [cm^3/g]	0.2668
V_{mes} [cm^3/g]	0.2559
D_{avg} [nm]	18.453
D_p [nm]	7.52

Figure 5.10 N_2 adsorption-desorption isotherm of synthesized CNPs

(■) Adsorption and (●) Desorption
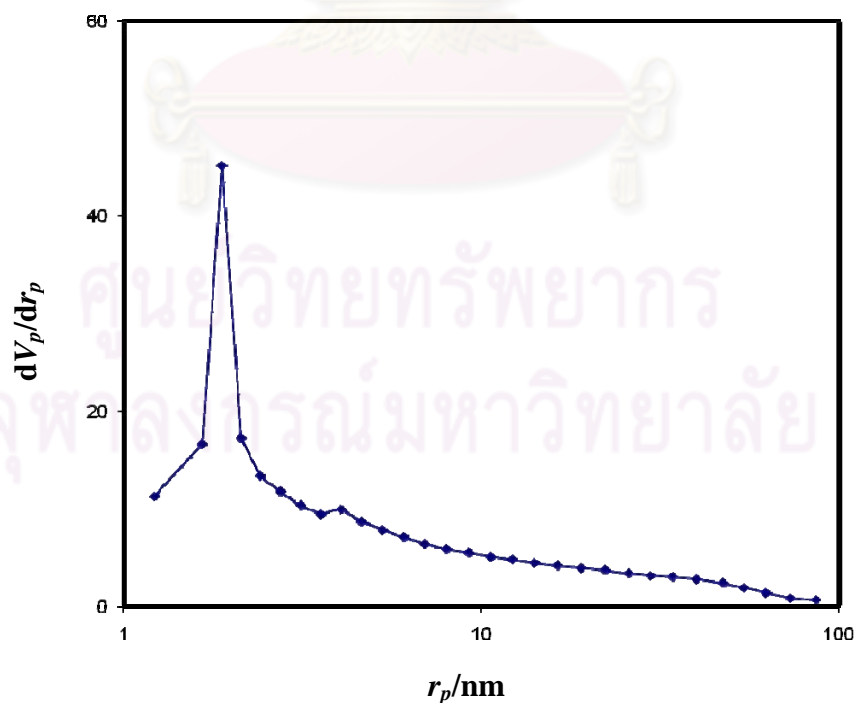
Figure 5.11 The pore size radius distribution

5.2 Effect of operating variables on dye adsorption performance

In this study, the adsorption efficiencies are investigated. Aqueous solution of Methylene Blue (C.I. Basic Blue 9, MB), Benefix Black B (C.I. Reactive Black 5, B5) and Benecion Red H8B (C.I. Reactive Red 31, R31) are used for all adsorption experiment. All batch adsorption experiments were analyzed with a UV-vis 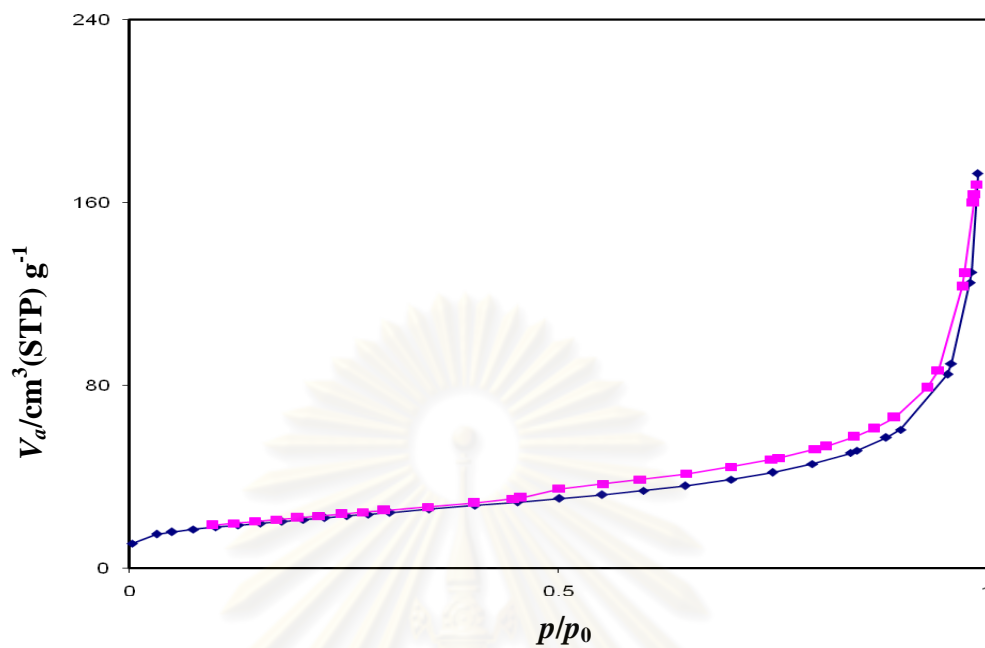spectrophotometer (UV-1700PC, Japan) at appropriate wavelength corresponding to the maximum absorbance (λ_{max}) of 664, 595 and 540 nm for MB, B5 and R31, respectively. The amount of dye adsorbed per unit mass adsorbent was calculated by the equation 5.1.

$$Q_t = \frac{C_0 - C_t}{W} V \qquad (5.1)$$

Where Q_t (mg/g) is the amount of dye adsorbed per unit mass adsorbent at any time t, C_0 (mg/L) is the initial dye concentration, C_t (mg/L) is the dye concentration at any time t(min), V (L) is the volume of solution and W (g) is the weight of the CNPs.

If adsorption is reversible and the adsorption and desorption rates equal each other for the system to be steady state. In this case, the steady state, which are assumed that is a well-mixed condition by the concentration profile, is also an equilibrium state because there are no net molecular fluxes. Therefore, Q_e (mg/g) and C_e (mg/l) are the amount of equilibrium dye adsorbed per unit mass adsorbent and the equilibrium dye concentration [30]. The united state environmental protection agency also suggested that the equilibrium state should be the time needed to establish a rate of change of the solute concentration in solution equal to or less than 5% per a day. [31].

5.2.1 Effect of contact time

Figure 5.12 presents the adsorption performance on CNPs as function of contact time. The effect of contact time on the removal of MB, B5 and R31 with the initial concentration of 40 mg/L, initial pH value of 6 and quantity of initial CNP adsorbents of 0.5 g/L are carried out. As explaining in 4.4, suspension of synthesized CNPs in solution of each dye solution was subject to ultrasonicated for 10 minutes.

Immediately after sonication, 10 ml of solution was sampled for detecting the amount of remaining dye.

(a)

(b)
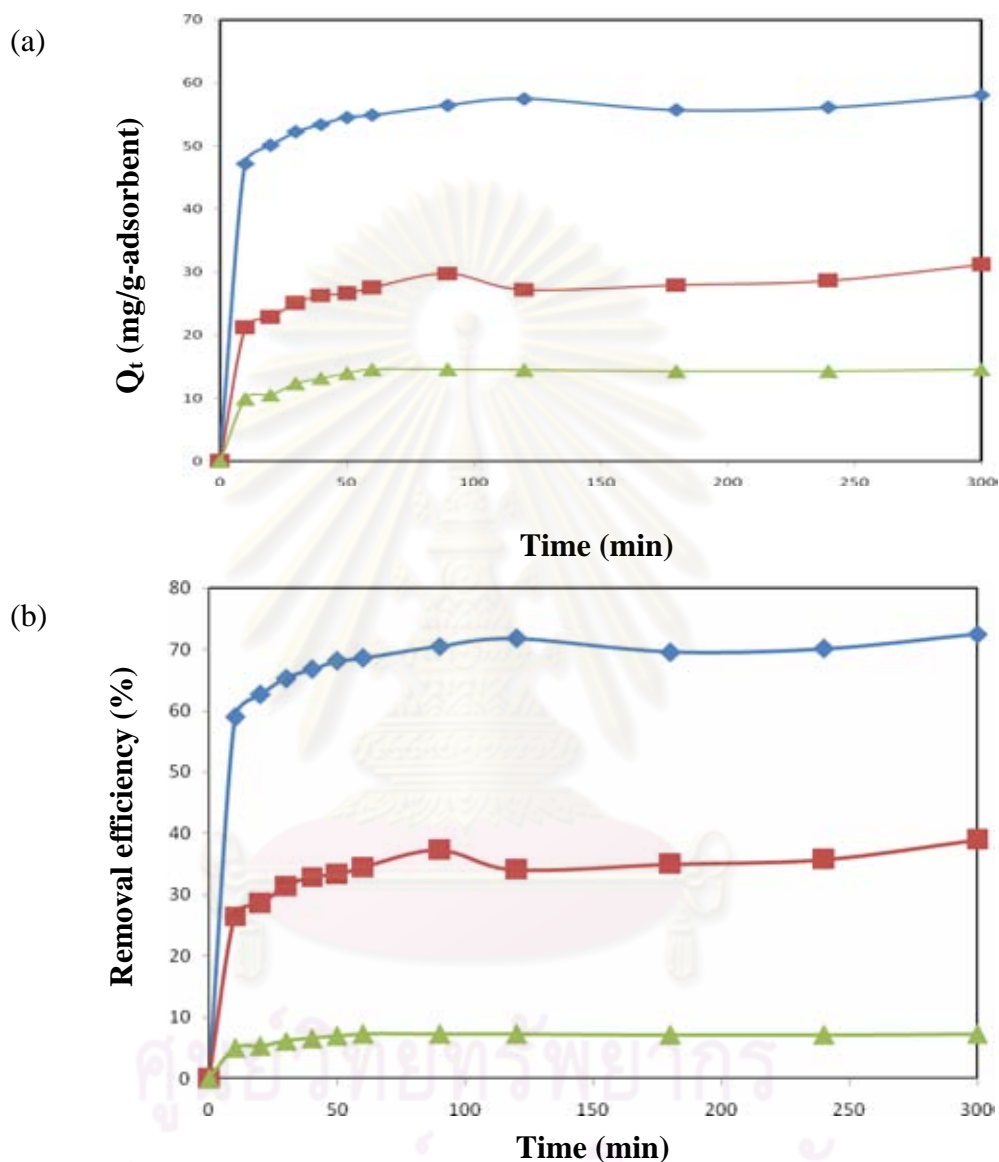
Figure 5.12 Plots of (a) amount of dye adsorbed and (b) removal efficiency of
(▲)MB, (♦)B5 and (■)R31 as a function of time

A rapid uptake of the dye adsorbed by synthesized CNPs occurred within a short time period followed by a slower stage until 60 minutes. After 60 min, no significant concentration change was found. Regardless of dye type, a rapid decrease in the concentration of dye remaining in the solution could be observed. It would be

reasonable to imply that all results represent a consistent trend of dye removal with respect to contact time. Similar observations could be found in literature. Luo et al. [26], who utilized halloysite nanotubes to adsorb Neutral Red (NR), suggested that the amount of NR adsorbed increased with the increase in contact time and reach the equilibrium within 30 minutes. Similar results were also obtained for adsorption MB and NR onto MWCNTs filled with Fe_2O_3 particles by Qu et al. [15] and for removal Brilliant Green onto carbon/iron oxide nanocomposite Ahmad and Kumar [27]. In addition, based on these results, further investigation would be conducted with respect to a constant contact time of 300 min.

5.2.2 Effect of initial dye concentration

The effect of initial dye concentration was inestigated in the range of 10 to 100 mg/L and 0.5 g/L CNPs loading at 25 °C for 6 hours. Figure 5.13 show plot of the removal efficiency versus initial dye concentration.
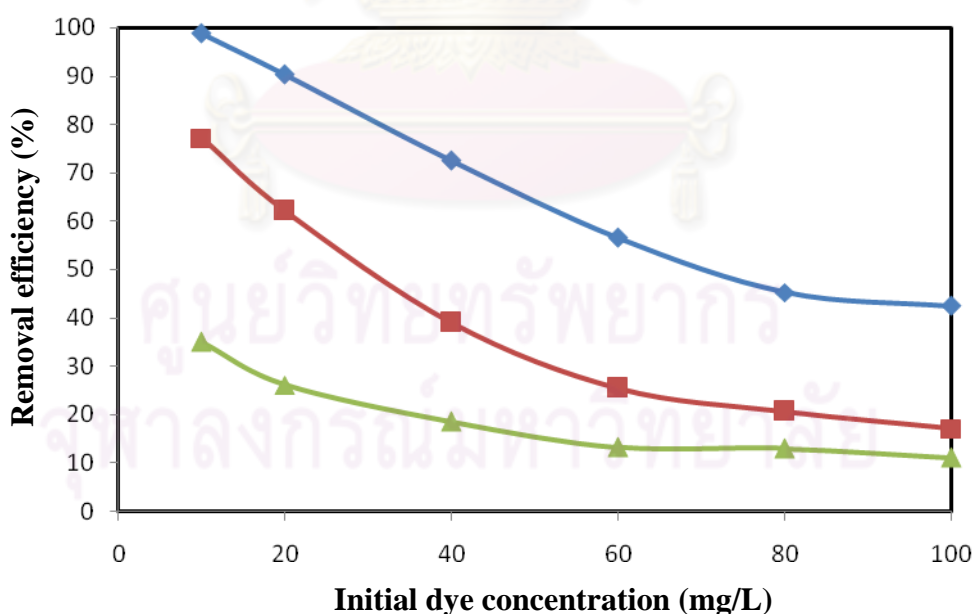
Figure 5.13 Plots of removal efficiency versus initial dye concentration:
(▲)MB, (♦)B5 and (■)R31

When the initial concentration increased from 10 to 100 mg/L, the removal efficiency decreased from 98.77 % to 42.47 %, 77.13 % to 17.13 % and 34.99 % to 11.05 % for B5, R31 and MB, respectively. The similar results can be observed by Amin [28], Therani-Banga et al. [33] and Shu [34]. Base on these result, it would be reasonable to imply that the initial dye concentration is one of an important factor in adsorption capacity of MB, B5 and R31 on synthesized CNPs.

5.2.3 Effect of the amount of CNPs loading

The amount of adsorbent loading is an important parameter in the determination of adsorption capacity. The effect of the amount of CNPs loading was investigated in the range from 0.3 g/L to 0.9 g/L with a constant of initial dye concentration of 60 mg/L and initial pH value of 6.
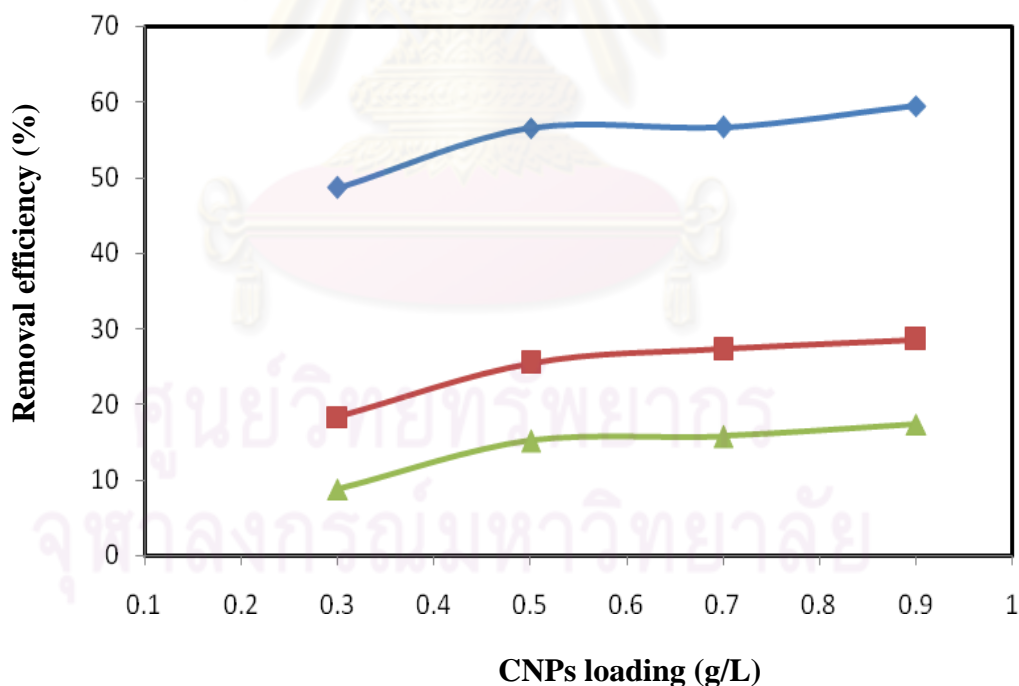
Figure 5.14 Plots of removal efficiency versus the amount of CNPs adsorbent:
(▲)MB, (♦)B5 and (■)R31

Figure 5.14 presents the removal efficiency increased with increasing of the dose of CNPs. However, they were not significantly altered beyond CNPs loading of 0.5 g/L. From the result, it suggested that increasing the CNPs dose increases the available active site on surface, leading to increase the adsorption on the available adsorbent surface. However, increasing of CNPs loading might increase the probability of the entanglement and agglomeration of CNPs, leading to decrease the adsorption on the overlapped external surface. The similar results can be observed by Amin [28], who utilized activated carbon from sugarcane bagasse pith to removal reactive dye in aqueous solution. The similar result was also obtained from Kuo et al. [18] and Luo et al. [26]. Based on these results, further investigation would be conducted with respect to a constant CNPs loading of 0.5 g/L.

5.2.4 Effect of initial pH value

The effect of initial pH value on adsorption efficiency experiments were studied over a range from 3 to 11 ($\pm$0.2). The experiments were carried out with initial dye concentration of 100 mg/L and 0.5 mg/L adsorbent. The results are shown in figure 5.15. It was observed that B5 and R31 removal efficiency decreased when pH value increased. The result may be explained by the electrostatic attraction between charged surface of CNPs and dyes.

As the zeta potential result in figure 5.9, when solution pH decreased, enhancing the electrostatic attraction between negative charged dye anions and positively charged surface of CNTs. Therefore, the removal efficiency of B5 and R31 was relatively high when the solution pH was below pH_{zpc}.

On the other hand, MB adsorbed is not significantly altered. MB is basic dye which can be classified as cationic dyes. It was observed that MB adsorbed increased with increasing pH value from 3 to 5 and then decreased slightly with further increasing pH value from 5 to 7. With further increasing pH value, MB adsorbed is not significantly changed. In pH range of 7 to 11, MB removal are higher than pH of 3, it might be from increasing the number of electrostatic attraction between the positively charged cationic dyes and negatively charged CNPs sites.
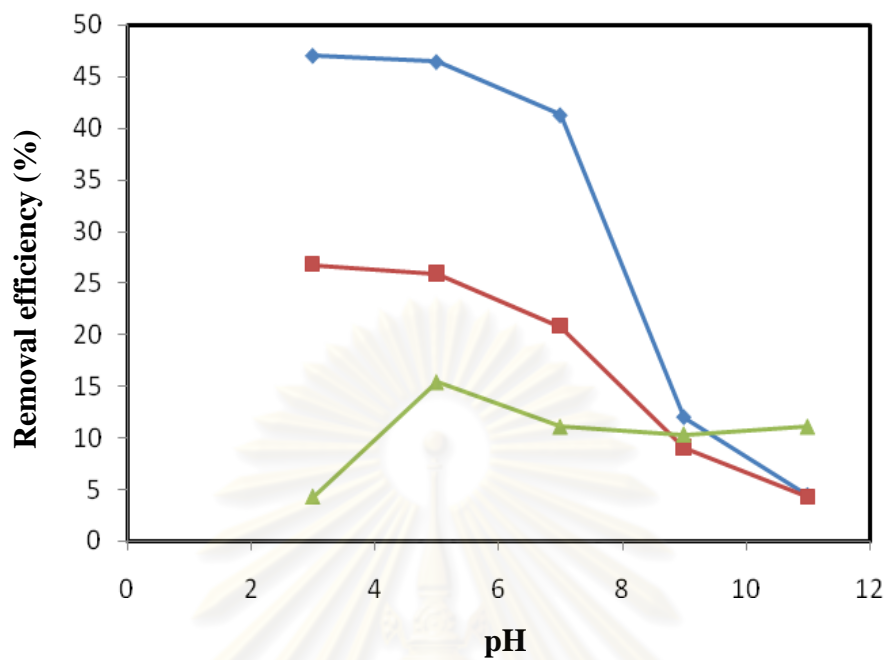
Figure 5.15 Effect of initial pH value of the solution on the adsorption of
(▲)MB, (♦)B5 and (■)R31 (C_0=100 mg/L, 0.5 g/L CNPs and contact time = 5 h.)

5.3 Adsorption isotherm

On the adsorption experiment, the adsorption isotherms for Methylene blue (MB), Reactive B5 and Reactive Red31 at a constant temperature of 25 ($\pm$ 2) °C was displayed in figure 5.16, which plot the relationships between the amount of dye adsorbed per unit mass adsorbent (Q_e) and the equilibrium concentration (C_e). The maximum adsorption capacities are 22.11, 34.26 and 84.94 mg/g for MB, R31 and B5, respectively. The experiment data were also analyzed with Langmuir and Freundlich isotherm models.
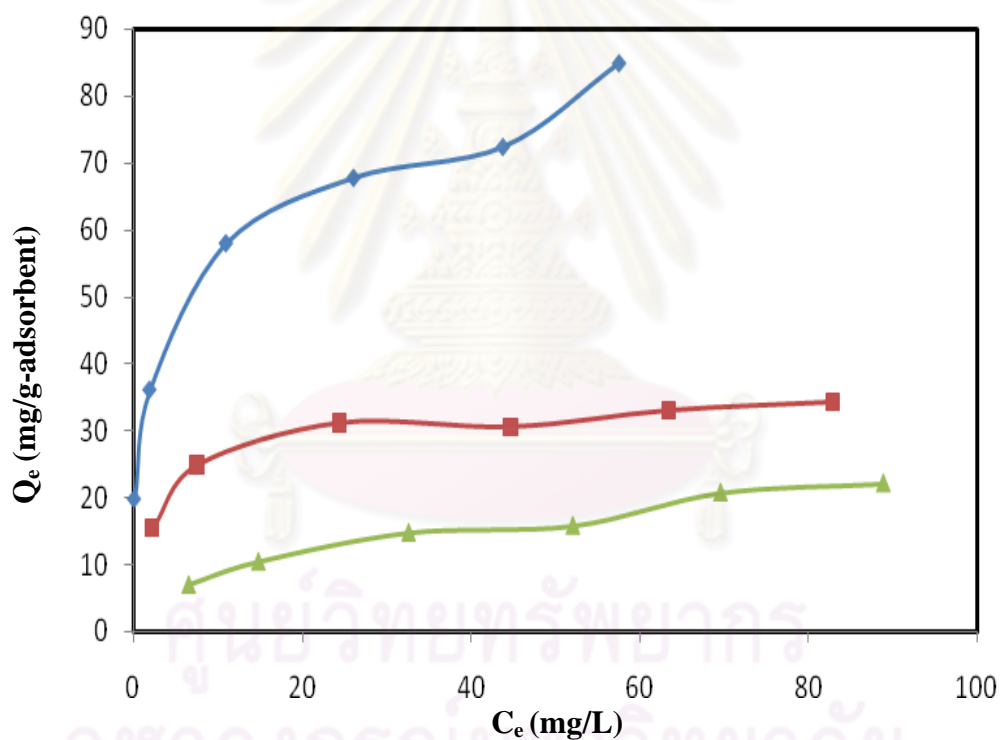
Figure 5.16 Adsorption isotherm of different typical dye at 25 °C:
(▲)MB, (♦)B5 and (■)R31

From the results, the sharp knee and the isotherm curve for B5, R31 and MB dyes indicates that the adsorption is favorable. In order to confirm the adsorption mechanism, Langmuir and Freundlich isotherms were used to describe the mechanism of the dye adsorption on CNPs.

The Langmuir isotherm model (From Eq.3.1 and 3.2) was chosen for estimation of the maximum adsorption capacity corresponding to complete monolayer coverage on the adsorbent surface. The adsorption isotherm of typical dyes on CNPs at 25 ($\pm$ 2) °C, which revealed the relationship between C_e/Q_e and C_e was fitted with the data of Langmuir model as shown in figure 5.17.
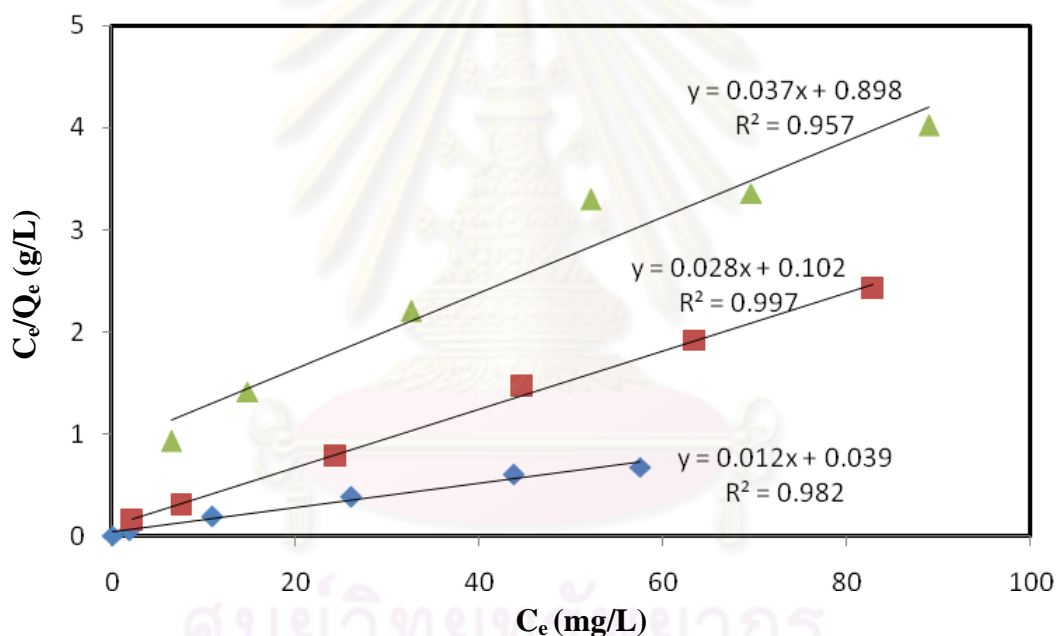
Figure 5.17 Langmuir plots for the adsorption of typical dye at 25 °C: (▲)MB, (♦)B5 and (■)R31

The Freundlich isotherm model (From Eq.3.3 and 3.4) was also chosen for describe the dye adsorption mechanism. Figure 5.18 displays the adsorption isotherm was fitted with the data of Freundlich model.
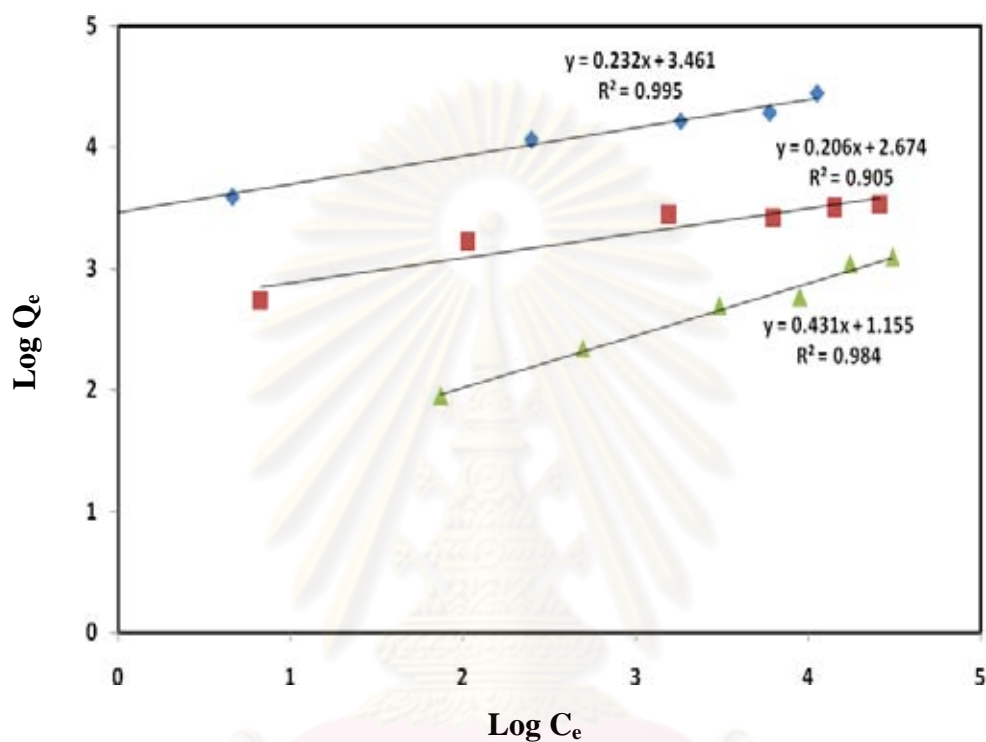
Figure 5.18 Freundlich plots for the adsorption of typical dye at 25 °C:
(▲)MB, (♦)B5 and (■)R31

Table 5.2 Constant values of Langmuir and Freundlich isotherms for dye adsorption onto CNPs at 25 °C

Dye	Langmuir				Freundlich		
	Q_m (mg/g)	K_L (L/mg)	R_L	r^2	K_F $(mg/g(mg/L)^{1/n})$	$1/n$	r^2
B5	83.333	0.308	0.0315-0.245	0.982	31.842	0.232	0.995
R31	35.714	0.275	0.035-0.267	0.997	14.488	0.206	0.905
MB	27.027	0.041	0.195-0.708	0.957	3.177	0.431	0.984

Table 5.2 summarized the coefficients of the Langmuir and Freundlich isotherms at 25 °C. Most of the r^2 values exceed 0.9. Based on the correlation coefficients (r^2), the experiment data of B5 and MB well fitted with Freundlich model and the experiment data of R31 well correlated with the Langmuir model. The lower Langmuir and Freundlich constant value (K_L and K_F) of the MB shows the weaker attraction toward the site of CNPs charge. K_L and K_F also indicates that the adsorption rate constant to desorption rate constant.

R_L lied between zero and unity, suggesting that the sorption is favorable for B5, R31 and MB on CNPs. The R_L values indicate that sorption is more favorable for the higher initial concentrations than for the lower ones. The sorption is very favorable for B5 and R31 and favorable MB. According to this classification, system favor ability tends to be in the order of B5 > R31 > MB.

Jiang et al. suggested that if $1/n$ less than unity, then the adsorption is physical; otherwise, the adsorption is chemical [29]. All values of $1/n$ less than 0.45, it would be reasonable to imply that the adsorption of three typical dyes in this study on synthesized CNPs is physical.

5.4 Kinetic model

In order to examine the mechanism and rate-controlling step, three kinetic models, pseudo first-order, pseudo second-order and intraparticle diffusion, are adopted to investigate the adsorption process with condition of initial dye concentration of 40 mg/l, CNPs loading of 0.5 g/L and initial pH value of 6.

Pseudo first-order equation:

$$\frac{dQ_e}{dt} = k_1(Q_e - Q_t) \tag{5.2}$$

From above equation, integrating it for the boundary condition $t = 0$ to $t = t$ and $Qt = 0$ to $Qt = Qt$, it may be rearranged for linearized data plotting as shown below:

$$\ln(Q_e - Q_t) = \ln(Q_e) - k_1 t \tag{5.3}$$

where Q_e and Q_t are the adsorption capacity at equilibrium and time t(min), respectively, and k_1 (min^{-1}) is the rate constant of the pseudo first-order

Pseudo second-order equation:

$$\frac{dQ_e}{dt} = k_2(Q_e - Q_t)^2 \tag{5.4}$$

Integrating this for the boundary conditions $t = 0$ to $t = t$ and $Qt = 0$ to $Qt = Qt$, which is the integrated rate law for a pseudo second-order model and can be rearranged to obtain:

$$\frac{t}{Q_t} = \frac{1}{k_2 Q_e^2} + \frac{1}{Q_e} t \tag{5.5}$$

where k_2 (g/mg.min) is the second-order rate constant. The initial adsorption rate h (mg/g min) can be determined from $h = k_2 q_e^2$.

Intraparticle diffusion equation: $\qquad Q_t = k_p t^{1/2} + C$

where k_p (mg/g.min$^{1/2}$) is the intraparticle diffusion rate constant.

Table 5.3 Coefficients of pseudo first-order kinetic model

Dye	Pseudo first-order			
	$Q_{e,\,exp}$ (mg/g)	$Q_{e,\,cal}$ (mg/g)	K_1 (min^{-1})	r^2
B5	58.020	5.883	0.007	0.414
R31	31.154	6.303	0.004	0.393
MB	14.567	1.590	0.022	0.277

Table 5.4 Coefficients of pseudo second-order kinetic model

Dye	Pseudo second-order				
	$Q_{e,\,exp}$ (mg/g)	$Q_{e,cal}$ (mg/g)	K_2 (g/mg.min)	h (mg/g min)	r^2
B5	58.020	58.824	0.0056	19.231	0.999
R31	31.154	31.250	0.0042	4.115	0.995
MB	14.567	14.925	0.0162	3.610	0.999

Table 5.5 Coefficients of intraparticle diffusion model

Dye	Intraparticle diffusion	
	K_p (mg/g.min$^{1/2}$)	r^2
B5	1.458	0.946
R31	1.360	0.981
MB	0.843	0.896

From the results, the pseudo first-order is not well fitted for B5, R31 and MB. Moreover, all of the calculated values of $Q_{e,cal}$ (mg/g) are far from the experimental values $Q_{e,exp}$ (mg/g). So the psuedo first-order kinetic model is not suitable to discribe the adsorption process as shown in figure 5.19.
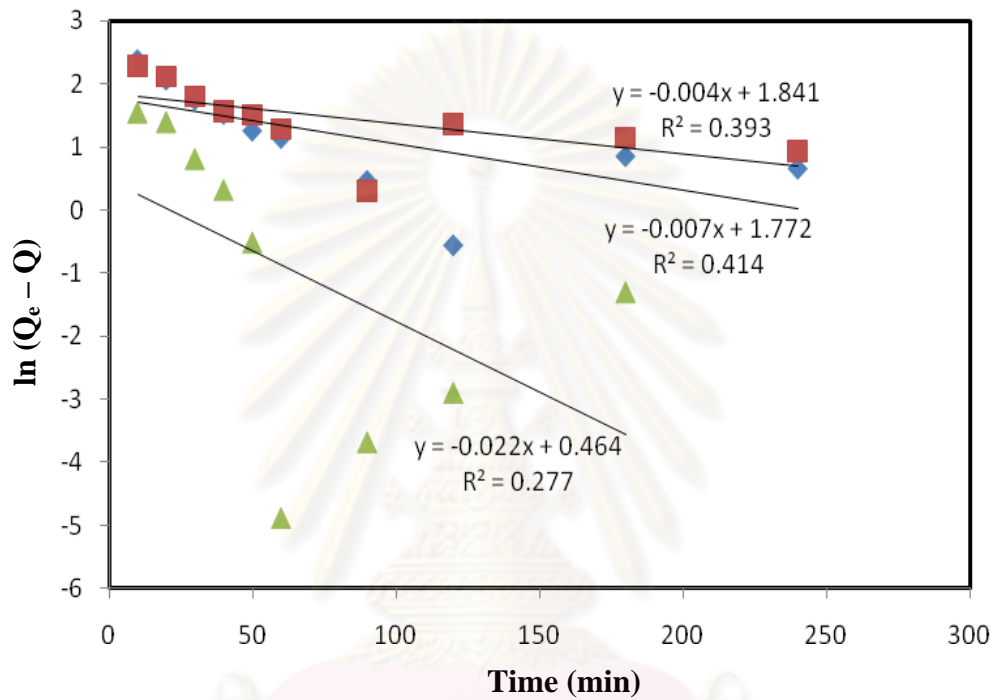
Figure 5.19 Regression of pseudo first-order model of
(▲)MB, (♦)B5 and (■)R31:
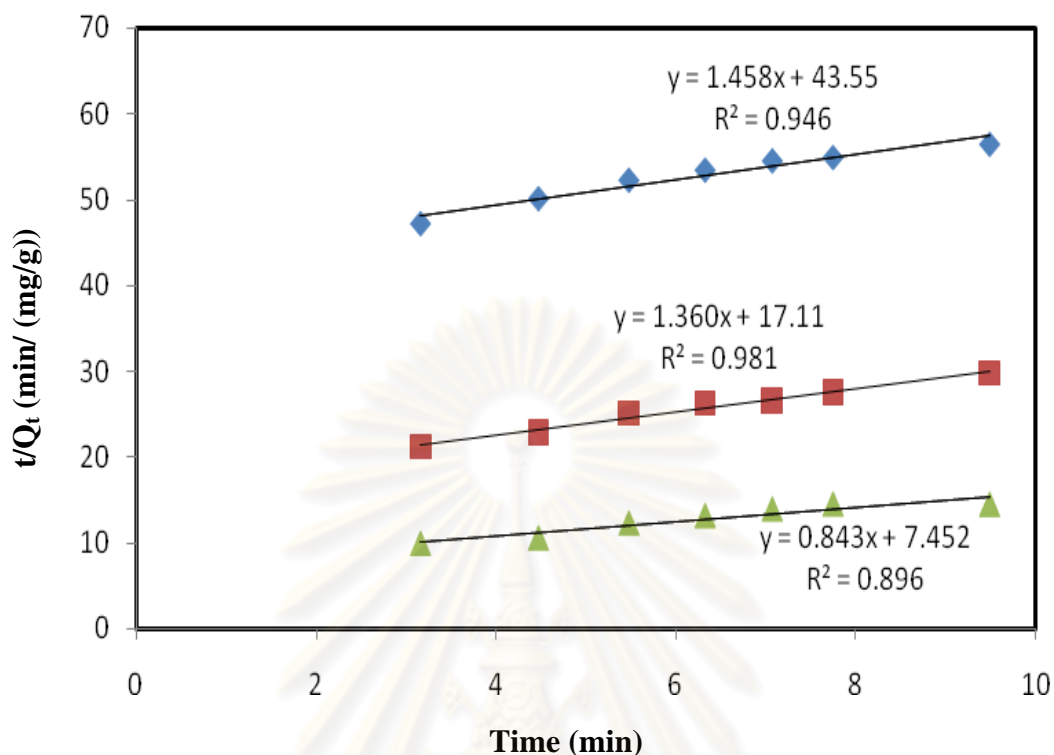
Figure 5.20 Regression of pseudo second-order model of
(▲)MB, (♦)B5 and (■)R31

However, regression of pseudo second-order was linear with the correlation coefficients (r^2) higher than 0.99. Furthermore, the calculated values of $Qe_{,cal}$ (mg/g) was consistent with the experimental values $Qe_{,exp}$ (mg/g). This study indicated that the psuedo second-order model can describe the adsorption process well as shown in figure 5.20.

Generally, the adsorption process on porous adsorbents has four steps. First step is external diffusion. The second step is film diffusion. The third is intra particle diffusion and the last step is finally adsorption of the solute onto the surface. Because neither the pseudo first-order nor pseudo second-order model can identify the diffusion mechanism during the adsorption process, the experimental data were analyzed by the intraparticle diffusion model for explain the diffusion mechanism.
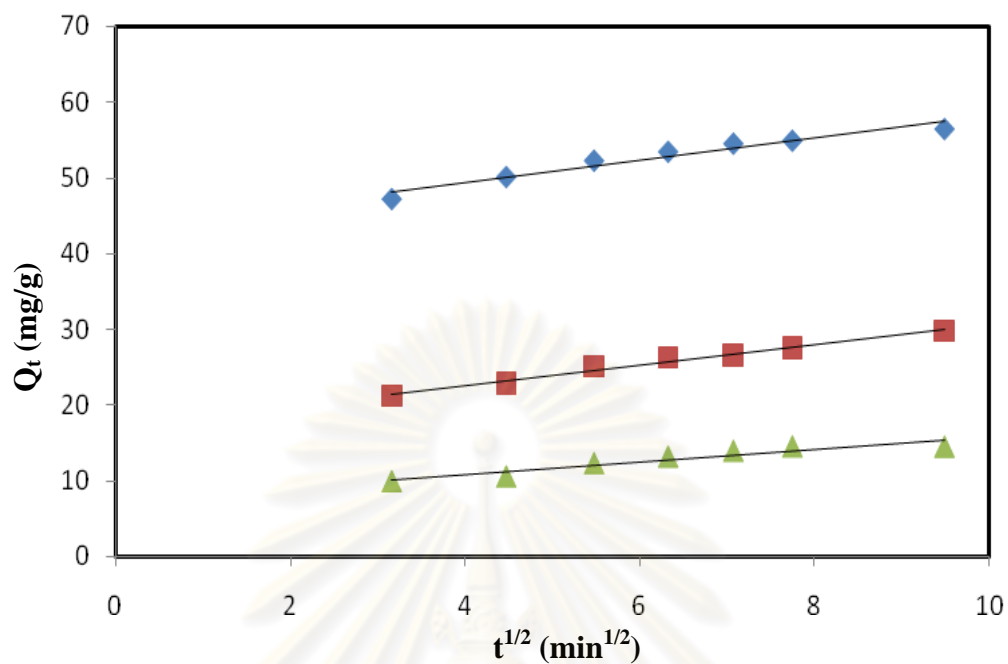
Figure 5.21 Regression of intraparticle diffusion model of
(▲)MB, (♦)B5 and (■)R31:

For the intraparticle model, film diffusion was negligible and intraparticle diffusion was the only rate-controlling step. Although the regression of q versus $t^{1/2}$ within a range of time less than 60 minutes was linear as shown in figure 5.21, suggesting that the adsorption would partially relate with intra-particle diffusion.

5.5 Desorption and regeneration of exhausted CNPs

The condition of desorption experiment are initial dye concentration of 100 mg/l, 0.5 g/l adsorbent and 24 hours of adsorption time at 25 °C and the initial pH value of 6. All experiments use NaOH and HCl to adjust the pH solution. After adsorption, adsorbents were seperated from the solution by eternal magnetic and filter membrane (0.45 µm), and oven-dried at 80 °C to a constant mass. The solution was measured the concentration with UV-spectrophotometer.

Exhausted CNPs were suspended in distillated water which was adjusted the pH value for 5 hours for regeneration. In this study, the range of initial pH value of the solution is 3-11. Re-adsorption experiment following the procedure described above for 3 cycles. The desorption efficiency was calculated by the follow equation:

$$\text{Desorption efficiency } (\%) = \frac{Q_e - Q_d}{Q_e} \times 100$$

Where Q_e and Q_d are the equilibrium adsorbed amount and residual adsorbed amount of the dye after desorption, respectively.

Figure 5.22 represents the variation of desorption efficiency of dyes with varied pH. It was observed that desorption efficiency of B5 and R31 increased when increasing pH of solvent. It has been found that when pH increases from 3 to 11, desorption efficiency of both of dye increases from 21.51 to 33.93% and 26.08 to 45.26% for B5 and R31, respectively. It might be said that R31 can desorbed easily than B5 because R31 (Molecular weight = 864) are smaller than B5 (Molecular weight = 993). For MB desorption, although the size of MB is smallest (Molecular weight = 320) but the maximum desorption efficiency is 13.80% at pH value of solvent of 11. It should be noted that pH of solvent are not affect to desorbs MB.
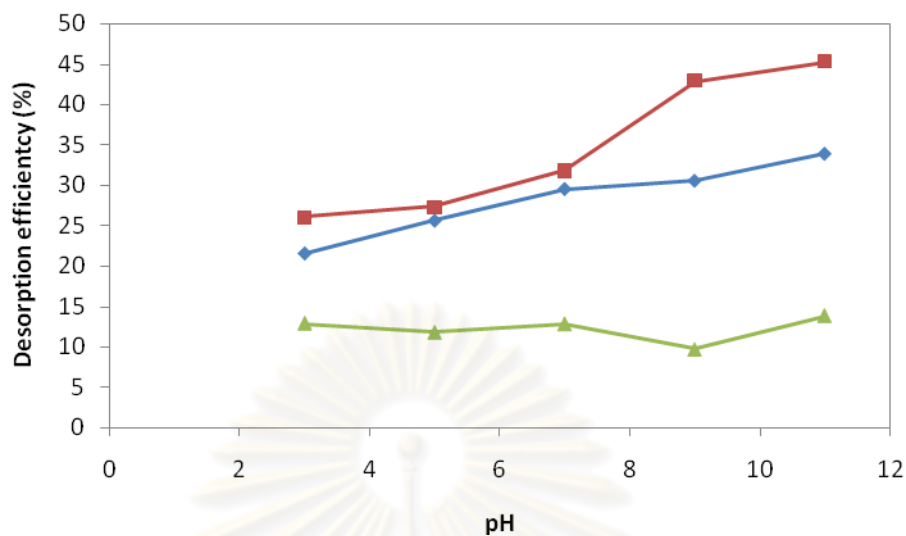
Figure 5.22 Effect of pH on desorption of exhausted CNPs

Over three adsorpton/desorption cycles, the re-adsorption efficiency result (as shown in Figure 5.23) was found that the loss in the sorption capacity between the first cycle and the last cycle was 33.07%, 48.99% and 19.97% for B5, R31 and MB, respectively.
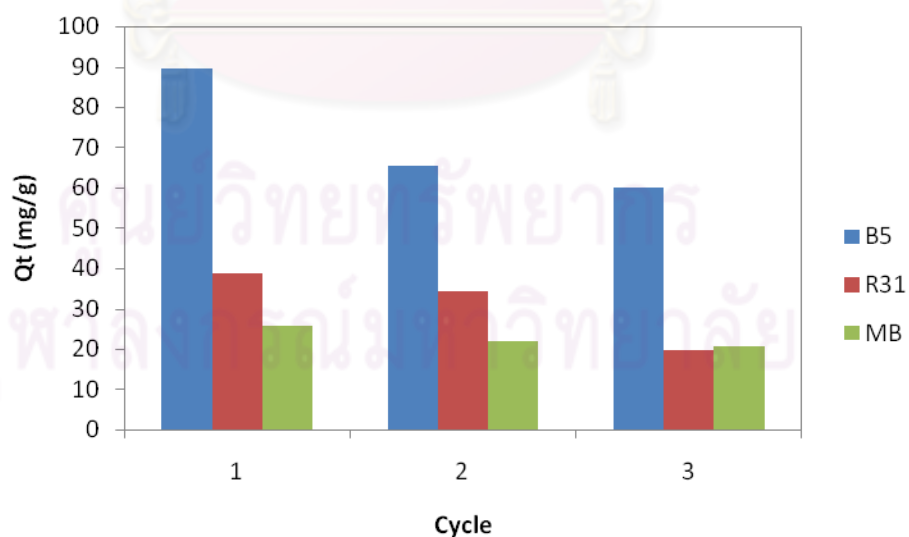
Figure 5.23 Sorption and re-adsorption of regenarate CNPs

5.6 Magnetic separation
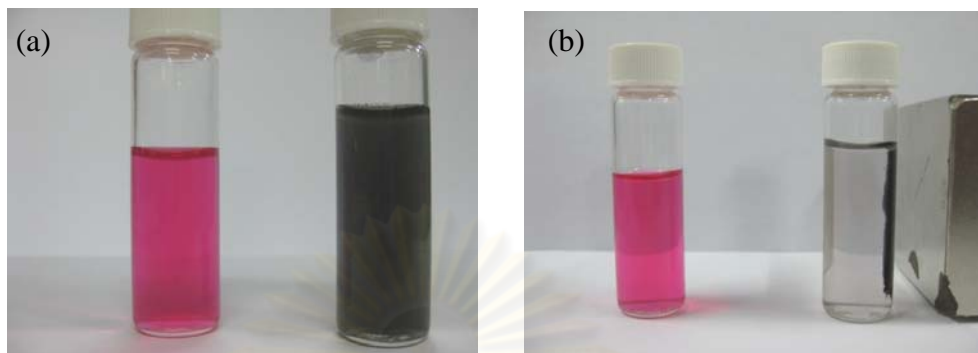
Figure 5.24 The magnetic separation: (a) suspension CNPs in aqueous dye solution and (b) CNPs attracted by external magnetic after adsorption process.

Figure 5.24 displays magnetic separation. In adsorption experiments, CNPs were suspended in aqueous solution as shown in figure 5.24 (a) for 5 h. After adsorption process, suspended CNPs were separated from the solution by external magnetic within 20 seconds as shown in figure 5.24 (b).
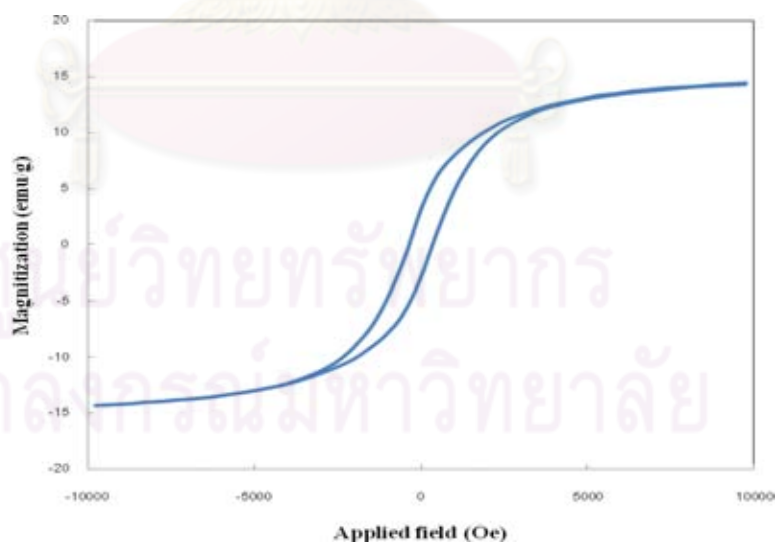
Figure 5.25 Magnetization curve of as-grown CNPs.

The hysteresis loop between ±10 kOe, which has a saturation magnetization of 14.25 emu/g (as shown in figure 5.25). The saturation magnetization of synthesized CNPs was higher than the other reported by Gong et al [16] and Zhu et al [20]. Based

on XRD results, the obtained CNPs showed the characteristic of ferromagnetism from bcc-Fe particles and superparamagnetism from fine Fe_2O_3 particles. The short time for CNPs separation from the solution after adsorption process exhibited high response rate with external magnetic field. Therefore, the synthesized CNPs are expected to be the novel solid adsorbent with the separation convenience process.

CHAPTER VI

CONCLUSION AND RECOMMENDATION

6.1 Conclusions

Carbon nanoparticles, including multi-walled carbon nanotubes (MWCNTs) and multi-shell carbon nanocapsules (CNCs), which are synthesized by co-pyrolysis of glycerol and ferrocene mixture with molar ratio of 5:1 at 900 °C have been utilized for Methylene blue, Reactive Black5 and Reactive Red31 removal. The main purpose of the research is to investigate the dye adsorption performance on synthesized CNPs. From the results, it can be concluded as follows:

6.1.1 Morphology and structure of CNPs

The obtained CNPs consist of multi-walled carbon nanotubes with diameters of 40-80 nm and multi-shell carbon nanocapsules. Moreover, the obtained products are multi-walled carbon nanotubes (MWCNTs) with iron particles filled in the tubes and at the tube tip and multi-shell carbon nanocapsules with iron particles which were encapsulated in the core. The BET specific surface area, total pore volume and average pore diameter were 73.85 m^2/g, 0.2668 cm^3/g and 18.453 nm, respectively.

6.1.2 Dye adsorption performance

This study investigated the removal of B5, R31 and MB from aqueous solution by synthesized CNPs. It takes only 60 minutes to reach the equilibrium. The amount of dye adsorbed per unit adsorbent mass increased with increases in the initial dye concentration but decreases as the increasing of adsorbent dose and initial pH value. R_L lied between zero and unity, suggesting that the adsorption of B5, R31 and MB on CNPs were favorable. The experiment data of B5 and MB well fitted with Freundlich model and the experiment data of R31 well correlated with the Langmuir

model. All values of $1/n$ less than 0.45, suggesting that the adsorption of three typical dyes in this study on CNPs is physical. Base on the regression of kinetic model, suggesting that the adsorption of B5, R31 and MB was best represented with the pseudo second-order model. Moreover, the results of kinetic analyses suggesting that the adsorption relate with intra-particle diffusion; however, that was not the only rate-controlling step. From the desorption experiment, It was observed that desorption efficiency of B5 and R31 increased when increasing pH of solvent. Over three adsorpton/desorption cycles, the re-adsorption efficiency result was found that the loss in the sorption capacity between the first cycle and the last cycle was 33.07%, 48.99% and 19.97% for B5, R31 and MB, respectively. The main advantage of the adsorption process on synthesized CNPs is its simplicity in the operation and recovery by magnetic system.

6.2 Recommendation for future work

From the experimental results, the batch adsorption performance of typical dye is investigated. The present work is the early step of revealing the formation of CNPs adsorbent and its adsorption mechanism. Surface modification of CNPs should be applied for more dye adsorption. For applied to large scale production, growth mechanism of CNPs, pilot-plant of dye removal and separation with external magnetic field should be studied for more details.

References

[1]   Iijima, S. Helical microtubules of graphitic carbon. <u>Nature</u> 354(6348) (1991): 56-58.

[2]   Sano, N., Charinpanitkul, T., Kanki, T. and Tanthapanichkoon, W. Controlled synthesis of carbon nanoparticles by arc in water method with forced convective jet. <u>J. Appl. Phys.</u> 96 (2004): 645-649.

[3]   Hou, H., Schaper, K.A., Weller, F. and Greiner, A. Carbon Nanotubes and Spheres Produced by Modified Ferrocene Pyrolysis. <u>Chem. Mater.</u> 14 (2002): 3990-3994.

[4]   Satishkumar, B.C., Govindaraj, A., Sen, R. and Rao, C.N.R. Single-walled nanotubes by the pyrolysis of acetylene-organometallic mixtures. <u>Phys. Lett.</u> 293 (1998): 47-52.

[5]   Lee, Y.T. and others. Temperature-dependent growth of carbon nanotubes by pyrolysis of ferrocene and acetylene in the range between 700 and 1000°C. <u>Chem. Phys. Lett.</u> 372 (2003): 853–859.

[6]   Satishkumar, B.C., Govindaraj, A. and Rao, C.N.R. Bundles of aligned carbon nanotubes obtained by the pyrolysis of ferrocene–hydrocarbon mixtures: role of the metal nanoparticles produced in situ. <u>Chem. Phys. Lett.</u> 307 (1999): 158-162.

[7]   Charinpanitkul, T., Sano, N., Puengjinda, P., Klanwan, J., Akrapattangkul, N. and Tanthapanichakoon, W. Naphthalene as an alternative carbon source for pyrolytic synthesis of carbon nanostructures. <u>J. Anal. Appl.</u> 86 (2009): 386-390.

[8]   Bai, S., Li, F., Yang, Q.H., Cheng, H.M. and Bai, J.B. Influences of ferrocene/benzene mole ration on the synthesis of carbon nanostructures. <u>Chem. Phys. Lett.</u> 376 (2003): 83-89.

[9]   Sano, N., Akazawa, H., Kikuchi, T. and Kanki, T. Separated synthesis of iron-included carbon nanocapsules and nanotubes by pyrolysis of ferrocene in pure hydrogen. Carbon 41 (2003): 2159-2179.

[10] Lu, Y., Zhu, Z. and Liu, Z. Carbon-encapsulated Fe nanoparticles from detonation-induced pyrolysis of ferrocene. Carbon 43 (2005): 369–374.

[11] Zhang, H., Liang, E., Ding, P. and Chao, M. Layered growth of aligned carbon nanotube arrays by pyrolysis. Physical B 337 (2003): 10–16.

[12] Kobayashi, M., Nakashima, H., Takagi, D. and Homma, Y. CVD growth of single-walled carbon nanotubes using size-controlled nanoparticle catalyst. Thin Solid Films 464–465 (2004): 286– 289.

[13] Li, D.C., Dai, L., Huang, S., Mau, A.W.H. and Wang, Z.L. Structure and growth of aligned carbon nanotube films by pyrolysis. Chem. Phys. Lett. 316 (2000): 349–355.

[14] Lee, Y.T. and others. Temperature-dependent growth of carbon nanotubes by pyrolysis of ferrocene and acetylene in the range between 700 and 1000°C. Chem. Phys. Lett. 372 (2003): 853–859.

[15] Qu, S., Huang, F., Yu, S., Chen, G. and Kong, J. Magnetic removal of dyes from aqueous solution using multi-walled carbon nanotubes filled with Fe_2O_3 particles. Jour. Hazard. Mater. 160 (2008): 643-647.

[16] Gong, J.L. and others. Removal of cationic dyes from aqueous solution using multi-walled carbon nanotube nanocomposite as adsorbent. Jour. Hazard. Mater. 164 (2009): 1517-1522.

[17] Wu, C.H. Adsorption of reactive dye onto carbon nanotubes: Equilibrium, kinetics and thermodynamics. Jour. Hazard. Mater. 144 (2007): 93-100.

[18] Kuo, C.Y., Wu, C.H. and Wu, J.Y. Adsorption of direct dyes onto carbon nanotubes: Determination of equilibrium, kinetics and thermodynamics parameters. Jour. Hazard. Mater. 327 (2008): 308-315.

[19] Luo, X. and Zhang, L. High effective adsorption of organic dyes on magnetic cellulose beads entrapping activated carbon. Jour. Hazard. Mater. 171 (2009): 340-347.

[20] Zhu, H.Y., Jiang, R., Xiao, L. and Zeng, G.M. Preparation, characterization, adsorption kinetics and thermodynamics of novel magnetic chitosan enwrapping nanosized γ-Fe$_2$O$_3$ and multi-walled carbon nanotubes with enhanced adsorption properties for methyl orange. Bioresource Technology. 101 (2010): 5063–5069.

[21] Kroto, H. W. and others. C60: Buckminsterfullerene. Nature 318(6042) (1985): 162-163.

[22] Terrones, M. Carbon nanotubes: synthesis and properties, electronic devices and other emerging applications.

[23] De Boer, J.H. The Structure and Properties of Porous Materials, Butterworths, London. IUPAC, Reporting Physisorption Data for Gas/Solid Systems, Pure Appl. Chem. 87 (1957): 603.

[24] Wu, F.C., Tseng, R.L. and Juang, R.S. Kinetic Modeling of Liquid-phase Adsorption of Reactive dyes and Metal ions on Chitosan. Wat. Res. 35(3) (2001): 613-618.

[25] Eckenfelder, W.W. Coagulation, Precipitation and Metals Removal. Industrial Water Pollution control, 3rd edn. Mcgraw-Hill, Boston. (2000): 124-157.

[26] Luo, P. and others. Study on the adsorption of Neutral Red from aqueous solution onto halloysite nanotubes. Wat. Res. 44 (2010): 1489-1497.

[27]   Ahmad, R. and Kumar, R. Kinetic and Thermodynamic Studies of Brilliant Green adsorption onto carbon/iron oxide nanocomposite. Jour. Korean Chem. Society. 54(1) (2010): 125-130.

[28]   Amin, N.K. Removal of reactive dye from aqueous solutions by adsorption onto activated carbons prepared from sugarcane bagasse pith. Desalination. 223 (2008): 152-161.

[29]   Jiang, J.Q., Cooper, C. and Ouki, S. Comparison of modified montmorillonite adsorbents. Part I: Preparation, characterization and phenol adsorption. Chemosphere. 47 (2002): 711-716.

[30]   Roy, W.R., Krapac, I.G., Chou, S.F.J. and Griffin, R.A. Batch-type procedures for estimating soil adsorption of chemicals. EPA project summary. (1992): 1-4.

[31]   Andrews, S.S. Accurate particle-based simulation of adsorption, desorption and partial transmission. Phys. Bio. 6 (2009): 1-15.

[32]   Langmuir, I. The adsorption of gases on plane surface of glass, mica and platinum. The research laboratory of general electric company. (1918): 1361-1403.

[33]   Tehrani-Bagna, A.R., Nikkar, N., Mahmoodi, N.M., Markazi, M. and Menger, F.M. The sorption of cationic dyes onto kaplin: Kinetic, isotherm and thermodynamic studies. Desalination. 266 (2011): 274-280.

[34]   Shu, H.Y., Chang, M.C., Chen, C.C. and Chen, P.E. Using resin support nano zero-valent iron particles for decoloration of acid blue 113 azo dye solution. Jour. Hazard. Mater. 184 (2010): 499-505.

[35]   Lu, P.J., Lin, H.C., Yu, W.T. and Chern, J.M. Chemical regeneration of activated carbon used for dye adsorption. Journal of Taiwan Institute of Chemical Engineers. 42 (2011): 305-311.

APPENDICES

APPENDIX A

Table A-1 Langmuir model data

Initial concentration	B5			
	Adsorbance	Conc. (ppm.)	qt (mg/g-adsorbent)	Ce/Qe
10	0.003	0.123	19.754	0.006
20	0.045	1.946	36.108	0.054
40	0.252	10.990	58.020	0.189
60	0.597	26.097	67.806	0.385
80	0.903	43.787	72.426	0.605
100	1.187	57.531	84.938	0.677
Initial concentration	R31			
	Adsorbance	Conc. (ppm.)	qt (mg/g-adsorbent)	Ce/Qe
10	0.042	2.287	15.426	0.148
20	0.140	7.572	24.856	0.305
40	0.452	24.423	31.154	0.784
60	0.828	44.721	30.558	1.463
80	1.146	63.483	33.034	1.922
100	1.496	82.870	34.260	2.419
Initial concentration	MB			
	Adsorbance	Conc. (ppm.)	qt (mg/g-adsorbent)	Ce/Qe
10	0.033	6.501	6.998	0.929
20	0.074	14.781	10.438	1.416
40	0.163	32.608	14.784	2.206
60	0.260	52.098	15.804	3.296
80	0.348	69.625	20.749	3.356
100	0.445	88.947	22.107	4.023

Table A-2 Freundlich model data

Initial concentration	B5				
	Adsorbance	Conc. (ppm.)	qt (mg/g)	log qe	log Ce
10	0.003	0.123	19.754	1.296	-0.91009489
20	0.045	1.946	36.108	1.558	0.28914283
40	0.252	10.990	58.020	1.764	1.04099769
60	0.597	26.097	67.806	1.831	1.41659058
80	0.903	43.787	72.426	1.860	1.64134654
100	1.187	57.531	84.938	1.929	1.75990355
Initial concentration	R31				
	Adsorbance	Conc. (ppm.)	qt (mg/g)	log qe	log Ce
10	0.042	2.287	15.426	1.188	0.35926616
20	0.140	7.572	24.856	1.395	0.87921060
40	0.452	24.423	31.154	1.494	1.38779900
60	0.828	44.721	30.558	1.485	1.65051150
80	1.146	63.483	33.034	1.519	1.80265906
100	1.496	82.870	34.260	1.535	1.91839779
Initial concentration	MB				
	Adsorbance	Conc. (ppm.)	qt (mg/g)	log qe	log Ce
10	0.033	6.501	6.998	0.845	0.81299486
20	0.074	14.781	10.438	1.019	1.16970969
40	0.163	32.608	14.784	1.170	1.51332149
60	0.260	52.098	15.804	1.199	1.71681938
80	0.348	69.625	20.749	1.317	1.84276770
100	0.445	88.947	22.107	1.345	1.94912935

APPENDIX B

International research papers

Publications Co-Authored by N. Akrapattangkul:

Charinpanitkul, T., Sano, N., Puengjinda, P., Klanwan, J., **Akrapattangkul, N.**, and Tanthapanichakoon W. Naphthalene as an alternative carbon source for pyrolytic synthesis of carbon nanostructures. Journal of Analytical and Applied Pyrolysis 86 (2009): 386-390.

Klanwan, J., **Akrapattangkul, N.**, Pavarajarn, V., Seto, T., Otani, Y., and Charinpanitkul, T. Single-step synthesis of MWCNT/ZnO nanocomposite using co-chemical vapor deposition method. Materials Letters 64 (2010): 80-82.

VITA

Mr. Nattapol Akrapattangkul was born in Songkhla, Thailand, on March 24, 1986. After completing his high-school level at Saengthong Vittaya school in Songkhla, in March 2004. He entered Prince of Songkla University, Songkhla, in June, 2004. After earning the degree of Bachelor of Engineering in Chemical Engineering in March, 2008, he gained admission to the Graduate School of Chulalongkorn University in June 2008. In April 2011, he was awarded the degree of Master of Engineering in Chemical Engineering with the thesis entitled "Removal dye pollutants using multi-walled carbon nanotubes with magnetic characteristics".